AD

SINGLE CRYSTAL CYLINDRICAL MAGNETIC DOMAIN MATERIALS FOR MEMORY APPLICATIONS

SEMIANNUAL TECHNICAL REPORT

By

D. M. Heinz, P. E. Elkins, P. K. George and B. J. Huffman

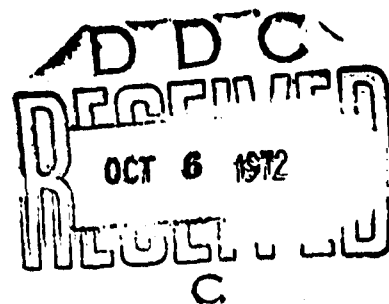September 1972

CONTRACT DAAB07-70-C-0258

Electronics Group
North American Rockwell
3370 Miraloma Ave, Anaheim, Calif. 92803

DDC

OCT 6 1972

C

ECOM

UNITED STATES ARMY ELECTRONICS COMMAND · FORT MONMOUTH, N.J.

AD 749267

NOTICES

Disclaimers

DOCUMENT CONTROL DATA - R & D

(Security classification of title, body of abstract and indexing annotation must be entered when the overall report is classified)

1 ORIGINATING ACTIVITY (Corporate author)	2a. REPORT SECURITY CLASSIFICATION
North American Rockwell Corporation Autonetics Division Anaheim, California 92803	Unclassified
	2b. GROUP None

3 REPORT TITLE

Single Crystal Cylindrical Magnetic Domain Materials for
Memory Applications

4 DESCRIPTIVE NOTES *(Type of report and inclusive dates)*
Semiannual Technical Report, 1 October 1971 to 30 May 1972

5 AUTHOR(S) *(First name, middle initial, last name)*

F. M. Heinz, P. E. Elkins, P. K. George, and B. J. Huffman

6 REPORT DATE	7a. TOTAL NO OF PAGES	7b. NO. OF REFS
September 1972	60	27

8a. CONTRACT OR GRANT NO. DAAB70-C-0258	9a. ORIGINATOR'S REPORT NUMBER(S) C70-1144.26/501
b. PROJECT NO.	
c. Task No. 1 HO-62101-A327 01.33	9b. OTHER REPORT NO(S) *(Any other numbers that may be assigned this report)* ECOM-0258-3
d.	

10. DISTRIBUTION STATEMENT

Approved for public release; distribution unlimited.

11. SUPPLEMENTARY NOTES	12. SPONSORING MILITARY ACTIVITY
None	U.S. Army Electronics Command Attn: AMSEL-TL-MA Fort Monmouth, N.J. 07703

13 ABSTRACT

The goal of this program is to demonstrate the feasibility of a buffer memory utilizing the controlled propagation of cylindrical magnetic (or bubble) domains. The bubble domain material investigation, directed toward preparing single crystal layers which exhibit useful device properties is being pursued with heteroepitaxial films of gallium-substituted yttrium iron garnet or related garnet compositions. The bubble domain device investigation is directed toward developing bubble manipulation techniques suitable for implementing the memory.

The body of the report contains sections on material and device work. The material section is chiefly concerned with Czochralski-grown rare earth garnet crystals used as substrates for bubble domain films. This discussion covers observed imperfections in crystals, the effect substrate imperfections have on bubble domain behavior in epitaxial films and crystal growth parameters which influence the formation of these imperfections. The device sections of this report present advances in bubble domain device physics and hardware. The discussion begins with a review of the results of calculations on bubble domain interactions with permalloy propagation patterns in a rotation magnetic field and then uses the conclusions to consider the problem of component design. A review is given on recent advances which have been made in the areas of propagation, generation, detection, annihilation and bubble switching.

This survey is followed by a discussion of the improvements which have been made in device fabrication, peripheral electronics and hardware. The report is concluded with a selected bibliography of journal articles pertinent to cylindrical magnetic domains.

KEY WORDS	LINK A		LINK B		LINK C	
	ROLE	WT	ROLE	WT	ROLE	WT
Cylindrical Magnetic Domains						
Bubble Domains						
Bubble Domain Device Components						
Bubble Domain Device Physics						
Crystal Growth						
Garnets						
Selected Bibliography						

SINGLE CRYSTAL CYLINDRICAL MAGNETIC DOMAIN MATERIALS FOR MEMORY APPLICATIONS

SEMIANNUAL TECHNICAL REPORT

1 October 1971 to 30 May 1972

CONTRACT NO. DAAB07-70-C-0258

Prepared by

D.M. Heinz, P.E. Elkins, P.K. George and B.J. Huffman

NORTH AMERICAN ROCKWELL

ELECTRONICS GROUP
ANAHEIM, CALIFORNIA 92803

For

U. S. ARMY ELECTRONICS COMMAND, FORT MONMOUTH, N. J.

DISTRIBUTION STATEMENT

Approved for public release;
distribution unlimited.

FOREWORD

The work described in this report is being carried out under Contract No. DAAB07-70-C-0258, Task No. 1HO-62101-A327 01.33 issued by Fort Monmouth Procurement Division, Procurement and Production Directorate, United States Army Electronics Command, Fort Monmouth, New Jersey 07703.

The Contract Monitor for this program is Mr. Thomas Collins, AMSEL-TL-MA, Applied Magnetics Team, USAECOM, Fort Monmouth, New Jersey.

The authors gratefully acknowledge the contributions of Dr. G. R. Pulliam, Dr. J. E. Mee, J. L. Archer, S. B. Austerman, Dr. P. J. Besser, A. G. Campbell, Dr. T. T. Chen, Dr. M. F. Ehman, Dr. H. L. Glass, E. F. Grubb, T. N. Hamilton, Dr. R. D. Henry, D. Kaneko, L. A. Moudy, Dr. L. R. Tocci, E. C. Whitcomb and J. L. Williams.

The following legend applies only to those pages so indicated in the subject report:

CONTENTS

ILLUSTRATIONS

TABLES

1. INTRODUCTION

This technical report is composed of three parts; first, an introductory section which presents the program goal; then, a review of material and device developments; and, finally, a summary of the status of the program.

The goal of this program is to demonstrate the feasibility of a buffer memory utilizing the controlled propagation of cylindrical magnetic (or bubble) domains. The bubble domain material investigation, directed toward preparing single crystal layers which exhibit useful device properties is being pursued with heteroepitaxial films of gallium-substituted yttrium iron garnet or related garnet compositions. The bubble domain device investigation is directed toward developing bubble manipulation techniques suitable for implementing the memory.

2. EXPERIMENTAL PROGRAM

This section deals with material and device developments since the last report[1]. Progress made in related areas on other programs is included so as to present a more complete picture of the status of bubble domain technology.

2.1 BUBBLE DOMAIN MATERIAL DEVELOPMENT

During the period covered by this report, the objective of work on materials has been to improve the properties of gallium-substituted yttrium iron garnet (GaYIG) films so as to make them useful in bubble domain devices. Of primary concern has been the elimination of film imperfections which impede bubble domain motion and serve as centers for unwanted generation or annihilation of bubble domains in a rotating magnetic field. The major experimental effort has centered on improvements in the quality of substrates.

2.1.1 Substrates

Bubble domain devices require a thin layer of single crystalline material which has an easy magnetization direction oriented perpendicular to its surface. This structure is conveniently obtained by epitaxial growth of a bubble domain composition on a nonmagnetic substrate. In films with stress-induced magnetic anisotropy, the substrate must (a) have a lattice parameter mismatch with the film that yields the proper amount of stress, and (b) provide the correct crystallographic orientation for the film so that the stress and magnetostriction constants produce an easy magnetization direction perpendicular to the surface. Earlier in this program, the objective was to attain the proper film-substrate lattice parameter mismatch to produce the necessary stress in the film[1,2]. More recently, the elimination of defects in films has become the major concern. Since an epitaxially-deposited film propagates the structure of the surface on which it is grown, except for accidental events during film growth, most film imperfections can be traced to the substrate crystal or its surface. This investigation has therefore been concerned with identification of the types and causes of imperfections in substrates and films so as to reduce their number. Inasmuch as related studies were being carried out on this and other programs, the efforts have been complementary and the net results are presented.

2.1.1.1 Substrate Crystal Imperfections

Imperfections within substrate crystals which have been identified with defects in epitaxial bubble domain films are (a) inhomogeneous elastic strains, (b) inclusions, (c) growth striations and (d) dislocations. In addition to being revealed by their effects on bubble domain behavior, these imperfections may be observed more directly by optical and X-ray diffraction techniques.

When a polished wafer is examined using transmitted linearly polarized light with the analyzer set for extinction, stress birefringence patterns such as are shown in Figure 1 reveal inhomogeneous strains in the wafers. The large central strain patterns on these (111) garnet wafers are associated with (211) facets at the solid-liquid interface of the growing substrate boule. There are also small, randomly distributed point defects in the central region of the wafer shown in Figure 1b. Under

a. Slice 17 from boule FM-14, (111) $Dy_{0.95}Gd_{2.05}Ga_5O_{12}$
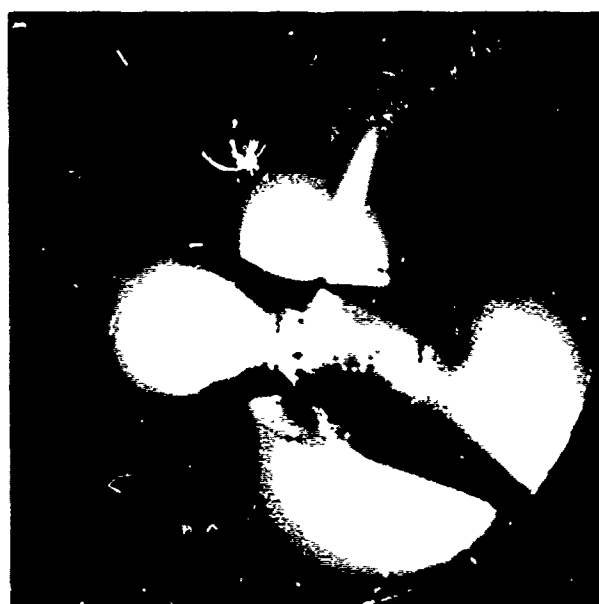
b. Slice 16 from boule NR-87, (111) $Dy_{0.95}Gd_{2.05}Ga_5O_{12}$

Figure 1. Patterns Revealed in Substrate Wafers by Transmitted
Polarized Light With Analyzer Set at Extinction (6.5X)

3

high magnification these points are revealed to be centered about opaque inclusions. Figure 2 shows one such inclusion about 10 μm in length which produces a strain pattern 30 times its size. These opaque inclusions are in the form of needles or platelets with triangular or hexagonal symmetry and may be larger or smaller than the one shown in Figure 2. Electron beam microprobe analysis has shown these particles to be iridium. Strain fields from iridium inclusions are propagated into epitaxial bubble domain films where they pin domain walls.

Microscopic examination of a wafer from near the seed end of a boule occasionally reveals the presence of microscopic voids as well as opaque iridium inclusions. The voids do not appear to have strain fields associated with them and only make their presence felt when the surface of a wafer intersects one, producing a pit. Other reported types of inclusions[3] have not been observed in these studies.

X-ray diffraction topography may also be employed to provide a photographic image of the imperfections in substrate wafers. Double-crystal asymmetric-reflection topography[4] was used to obtain Figure 3 using FeKα_1 radiation, (842) reflection. This topograph was made on the same wafer as was Figure 1a and the pictures reveal identical symmetry. Additional features are the boundaries to the central core "propeller" and growth striations. The striations form concentric circles except in the core region where they are approximately straight and parallel. Since contrast in an X-ray diffraction topograph is a manifestation of deviation from a perfectly periodic crystal, the striations reveal changes in lattice parameter. Due to the sensitivity to lattice parameter difference of this double-crystal topography technique, the core region in Figure 3 is white while the striations are in shades of black and grey. The difference in contrast indicates that the lattice parameter of the core region is different from that of the remainder of the wafer; typically the core lattice parameter is about 0.002Å greater. Thus in a general way, the topograph lattice parameter differences are related to the optical strain patterns. Fewer point defects are seen in Figure 3 than in Figure 1a. This is probably due to the fact that all inclusions within the bulk of the slice are made visible by the optical transmission technique while the X-ray reflection technique reveals only strain fields of inclusions which extend to within a few microns of the surface.

Topographs of gadolinium gallium garnet (GdGG) wafers exhibit growth striations which represent small deviations from the stoichiometric composition, $Gd_3Ga_5O_{12}$. Topographs of mixed dysprosium gadolinium gallium garnets (DyGdGG) such as are used as substrates for GaYIG, e.g., $Dy_{0.95}Gd_{2.05}Ga_5O_{12}$, have more pronounced growth striations which means that the lattice parameter variations are greater. Growth striations propagated into epitaxial bubble domain films have been observed to behave as barriers to bubble domain motion.

Another type of defect which can be propagated into an epitaxial bubble domain film and pin domain walls is the dislocation. When present in a wafer, this imperfection may be observed by employing increased magnification with the optical and X-ray techniques described above. Dislocations are revealed more readily by selective chemical etching but the surface finish is destroyed in the process. Figure 4 shows typical etch pits produced by immersion in phosphoric acid at 180°C for five minutes[5]. The point-bottomed pits define the sites of dislocation emergence. Pits marked A and B are two types of pits. Both are associated with dislocations but the reason for the differing geometries is not clear at this time. Some etch pits, such as the one marked

4
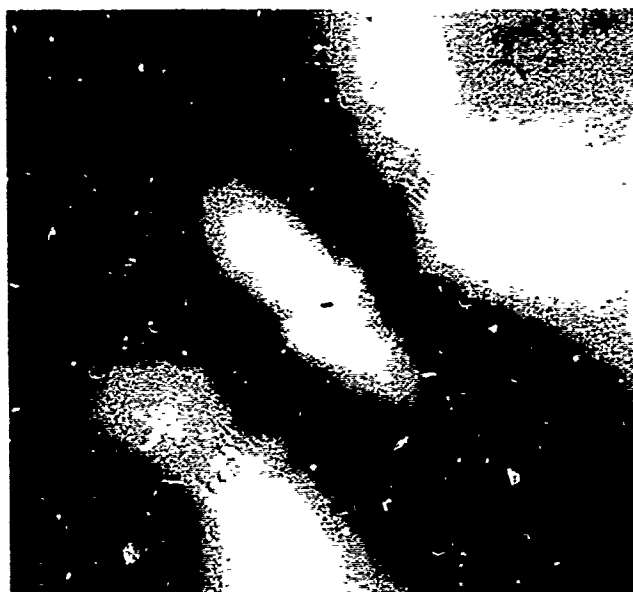
Figure 2. Iridium Inclusion and Strain Pattern Revealed in Substrate Wafer by
Transmitted Polarized Light With Analyzer Set at Extinction (194X)
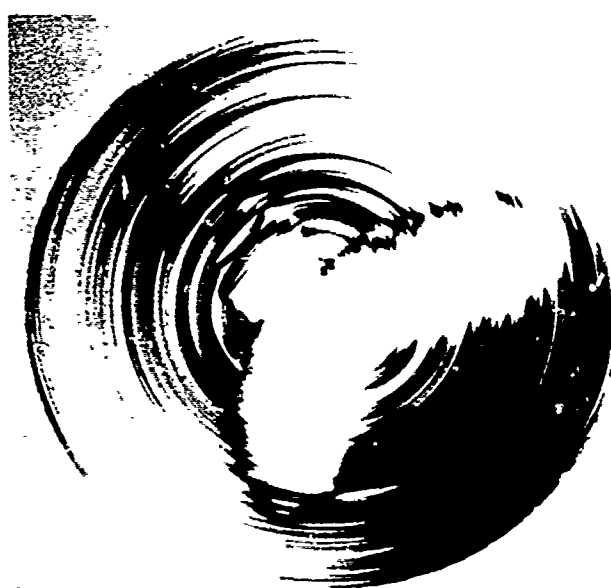
Slice 17 from boule FM-14, (111) $Dy_{0.95}Gd_{2.05}Ga_5O_{12}$

Figure 3. X-ray Diffraction Topograph of a Substrate Wafer (6.5X).
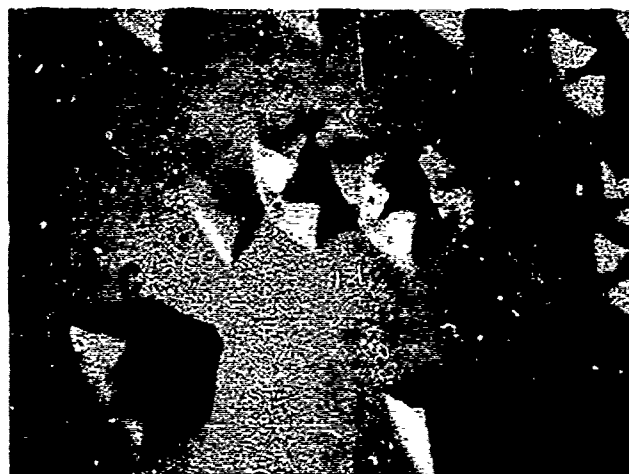
Slice 17 from boule FM-10, (111) $Dy_{0.95}Gd_{2.05}Ga_5O_{12}$

Figure 4. Etch Pits in a Substrate Wafer (630X).

C in the Figure, are the result of a cluster of dislocations as evidenced by the twin pits at the bottom. The flat-bottomed pit marked D in the Figure is typical of those which occur at point defects and surface damage.

Occasionally it is possible to observe etch pits produced on opposite faces of a wafer with the points of the pits aligned to define the trace of the dislocation. The density of dislocations on a wafer is generally highest near the center and near the periphery. The former are primarily growth-induced while the latter are commonly introduced by mechanical shaping of the boules during processing. Selective chemical etching also reveals growth striations on a wafer which are similar to those observed by X-ray topography.

The types of imperfections in Czochralski-grown rare earth garnets, means of observing them, and their effects on epitaxial bubble domain films are summarized in Table I.

Table I. Imperfections in Czochralski-Grown Rare Earth Garnets

Imperfection	Means of Observing	Effect on Epitaxial Bubble Domain Film
Dislocation	Selective chemical etch X-ray topography Polarizing microscope	Always detrimental – pins domain wall
Iridium inclusion	Polarizing microscope X-ray topography Selective chemical etch	Always detrimental – pins domain wall
Void	Microscope	Rarely detrimental – can form pit in surface
Growth Striation	X-ray topography Selective chemical etch	Occasionally detrimental – some behave as a barrier to bubble propagation.
Core	X-ray topography Polarizing microscope	No identified effect – lattice parameter difference may produce a barrier to bubble propagation.
Inhomogeneous Elastic Strain	Polarizing microscope	Inconvenience – stress birefringence occasionally interferes with viewing domains in portions of a film.

2.1.1.2 Substrate Crystal Growth

Improvement in the quality of GaYIG films begins with improving the quality of the DyGdGG substrates. Since the imperfections found in substrate wafers are directly dependent on the crystal growth conditions, it is here that improvements in the quality of substrate material may be made. In Czochralski crystal growth, the major growth parameters are rotation rate, pull rate, temperature gradients at the solid-melt interface, ratio of boule to crucible diameter, gaseous ambient and seed orientation. Selection of growth conditions which will reduce or eliminate the incidence of imperfections may be made after the influence of each growth parameter is understood. The following is our present understanding of the growth process based on observations of the occurrence of crystalline imperfections in rare earth gallium garnet boules.

Boule slices and longitudinal sections when viewed by transmitted linearly polarized light exhibit an overall pattern which is superimposed on a weaker pattern of striation bands. In a longitudinal section, the bands delineate the crystal growth interface as the boule was grown. Generally, at high rotation rates, the interface is convex toward the melt while the boule diameter is being established. The interface takes on a flat to concave shape as growth of a uniform diameter commences. The shape of the boule interface and the boule orientation determine the strain pattern as viewed by polarized light. In the garnet system, the <211> and <110> directions are slow growth directions. Therefore, facets develop on the growth interface where these pole directions intersect the growth interface at right angles. As the curvature of the interface is reduced, a point is reached where the <110> poles no longer intersect

7

the interface at right angles. At this point the strain and striation associated with the (110) facets disappear.

At sufficiently high rotation rates the interface becomes flat enough so that the <211> poles do not intersect the interface at right angles. At this point the interface is flat or slightly concave with respect to the melt. With a flat to slightly concave interface shape, no facets are observed to form in the bulk of the boule.

The pattern of strain that is revealed by polarized light is strongly related to the facets in boules grown with a convex interface. For (111) boule slices, the background of the pattern is light indicating that a considerable portion of the light is being depolarized by the slice before it passes through the analyzer. If (110) facets are present, a distinctive fringe in the shape of a cross is found at these facets. For boules grown at high rotation rates where the interface is flat to slightly concave, the boule slices are dark except at the edge of the boule. Here a bright region is found at the four locations corresponding to the (211) facets.

Growth striations are observed in Czochralski-grown rare earth gallium garnets as concentric bands in crystal slices with the boundary between bands sharply delineated. These bands represent slight compositional variations in the crystal. Temperature fluctuations can occur at the growth interface as a result of convection in the melt which produces slight cyclic changes in the rare earth to gallium ratio of the growing crystal. Thus, within each band the composition varies from that of the overall melt stoichiometry. The growth striations in a slice perpendicular to the growth axis can be minimized by growing a boule with a flat interface from a melt where convection is suppressed, e.g., by minimizing the axial temperature gradient in the melt.

Dislocations in Czochralski-grown rare earth garnets appear to result from independent growth accidents rather than to relieve strain during cooling as occurs in metals. They are observed to be of two types; those inclined at a large angle to the growth axis, and those aligned nearly colinear with the growth axis. The first type of dislocation is usually observed at the top of a boule in that portion where the boule diameter was being established. They result from the extremely high radial solidification rates that occur when one attempts to establish the boule diameter too quickly. These dislocations appear as radial lines or bands when the polished slides of the boule are observed under transmitted linearly polarized light. They usually disappear within the first centimeter of uniform boule diameter growth. Dislocations aligned with the boule axis (axial dislocation) usually occur when the growth interface becomes too concave toward the melt. Once they are introduced into the crystal, they persist as long as the growth interface remains flat to concave. Typically, the density of these axial dislocations ranges from 10 to 5,000/cm^2. Such dislocations can be reduced by controlling the shape of the interface so that it is flat to slightly concave. The growth parameter having the most influence on the interface shape is the rotation rate.

An equally severe defect found in the rare earth garnets is the presence of microscopic iridium metal inclusions. (The source of iridium is the crucible.) Two factors are responsible for the occurrence of iridium particles in a crystal: (a) a finite solubility of iridium in the garnet melt which increases with temperature and (b) convection in the garnet melt which pumps fluid from the hot bottom of the crucible

8

to the colder crystal interface and melt surface. Control and elimination of inclusions can be achieved by reducing the axial temperature gradient in the garnet melt.

The formation of voids is related to the amount of dissolved gas in the melt at the crystal interface. Since gases are more soluble in liquids than in solids, one may consider the nucleation of gas bubbles on the surface of a growing crystal when the crucible temperature is lowered abruptly. Such a situation creates a condition of supersaturation of dissolved gas because the crystal grows out rapidly and rejects dissolved gas. When the concentration of dissolved gas exceeds the solubility limit sufficiently, gas bubbles form and attach themselves to the growing crystal. Growth of the crystal around these bubbles then results in the formation of voids. The condition which prompts this change in solubility, growth at too rapid a rate, should be avoided.

The relative dimensions of the boule diameter and the crucible diameter play an important role in shaping the solid-liquid interface. This is a growth parameter which is undoubtedly interrelated with the temperature gradients and shear effects caused by rotational stirring. As the boule diameter increases relative to the crucible diameter, the interface becomes more convex favoring facet development. Growth of a larger diameter boule removes material from the melt more rapidly so that the level of liquid falls, possibly changing the thermal environment. Thus, for flatter interface development and less strain, the ratio of boule diameter to crucible diameter should not be large.

The growth of rare earth gallium garnets is complicated by the fact that they must be grown in an oxygen-containing atmosphere because trivalent gallium oxides decompose at the elevated crystal growth temperatures into a volatile suboxide, Ga_2O, and oxygen. On the other hand, the iridium crucibles are attacked by oxygen at these temperatures. It is therefore desirable to grow crystals in an ambient which contains the minimum amount of oxygen required to suppress loss of Ga_2O. Typically two to five percent oxygen in nitrogen has been used.

The seed orientation determines the relative positions of the facets at the growing crystal interface and hence influences the boule shape. However, it has little effect on imperfections and orientation selection is based on other factors.

For substrate applications, the most desirable boules would be completely free of dislocations, iridium particles, growth striations and facet strains. The factors that must be controlled to produce such optimum substrates are:

1. The axial and radial temperature gradient in the melt and in the growing crystal should be low.

2. The interface shape should be flat to slightly concave to reduce the development of facets and axial dislocations. The growth parameter having the greatest influence on the interface shape is the rotation rate of the crystal.

9

Table II contains a summary of observations and hypotheses on the effects of crystal growth parameters on Czochralski-grown rare earth garnet boules. Since the growth parameters are not completely independent, values for parameters must be compatible within the constraints of the equipment. The information has been collected from growth experiments on many GdGG crystals, a number of other rare earth gallium garnet crystals, several mixed rare earth gallium garnet crystals and several mixed aluminum-gallium garnet crystals. In general, the mixed garnet crystals behave like the simple garnets but the intensity of growth striations, core, and inhomogeneous strain is greater, and the occurrence of void formation is slightly increased for the same set of growth conditions. Several of these differences may be explained plausibly on the basis of a difference in solidus and liquidus for the mixed crystals.

As shown in Tables I and II, a number of imperfections have been identified and explanations offered for their occurrence in terms of crystal growth parameters. Core-free, low dislocation density ($<10/cm^2$) GdGG crystals have recently been grown. However, to improve crystal quality further, modifications in the crystal growth equipment must be made which will extend the range of control over the thermal environment at the solid-liquid interface. These modifications are underway.

2.1.1.3 Substrate Wafer Preparation

After a substrate crystal boule has been grown, it is ground to a standard diameter of 0.50 inch. The cylindrical crystal is next oriented along its <111> axis by X-ray back-reflection Laue techniques and sawed into 0.030 inch-thick wafers with an annular diamond saw. The slices are then lapped and polished flat and parallel on both sides using vibratory polishing machines. The lapping steps employ a series of loose alumina abrasives which vary from 12 to 3 μm and the polishing step employes Linde A (0.3 μm α-alumina). A final polish is performed on the wafer surface to be used for epitaxy employing Syton (a colloidal dispersion of silica in an alkaline medium). At the completion of this final polishing step, a flat is ground on the edge from the surface with the Linde A finish so as to distinguish between the sides of the wafer. A final cleaning with organic solvents is carried out to dissolve the wax which bonded the wafer to its polishing block and to dislodge dust particles. Some substrates are also subjected to a brief chemical polish etch in 300°C phosphoric acid[5] prior to epitaxial deposition. If a wafer is not used promptly following a final cleaning, it will probably be necessary to repeat the process to remove dust particles.

The surface of a substrate wafer must be properly prepared in order to prevent the generation of imperfections in an epitaxial bubble domain film. The sources of these imperfections may be (1) a damaged surface which is present due to inadequate polishing or mishandling, or (2) foreign material such as dust particles or a stain from a solvent which are present due to insufficient cleaning prior to deposition.

Table II. Effect of Czochralski Crystal Growth Parameters on Crystal Quality

Growth Parameter	Influence on Crystal Growth	Influence on Imperfections
Rotation rate	High rate favors flat to concave interface shape, eliminates facet development and increases stirring of melt.	High rate reduces dislocation density and inhomogeneous strain, eliminates core and increases iridium inclusion density.
Pull rate	High rate favors convex interface shape and facet development.	High rate increases void formation, dislocation density and inhomogeneous strain.
Temperature gradients at solid-liquid interface	Low gradient favors concave to flat interface shape, reduction of facet development and reduction of convection in melt.	Low gradient reduces dislocation density, iridium inclusion density, inhomogeneous strain and growth striations.
Ratio of boule to crucible diameter	Small ratio favors flat to concave interface shape and reduction of facet development.	Small ratio reduces dislocation density and inhomogeneous strain.
Gaseous ambient	High oxygen partial pressure favors oxidation of iridium crucible and suppresses loss of Ga_2O from melt.	None identified. May be able to find an inert gas of low solubility in melt to reduce void formation at high pull rates.
Seed orientation	Determines relative positions of facet development.	None identified.

11

Interference contrast microscopy and dark field microscopy are used to inspect wafers prior to film deposition. Damaged material must be completely removed or its presence will be revealed by the epitaxial deposit. X-ray diffraction topography studies have shown that the surface damage on a well-polished wafer extends approximately one μm below the surface. Selective chemical etching readily reveals work damage because strained material dissolves more readily than unstrained material. Figure 5 shows a garnet substrate which had been mechanically polished to a mirror finish, then lightly etched in a 1:1 phosphoric acid-sulfuric acid solution at 200°C for five minutes. The scratches which have been revealed are remnants of work damage which had not been completely removed during a prior lapping step.

Most of the substrate internal surface flaws can be identified by microscopic examination prior to film deposition. However, some imperfections escape detection until after a magnetic film has been deposited and the domains exercised. Figure 6 shows the domain pattern of a portion of a GaYIG film on DyGaGG substrate under low magnification with no applied magnetic field. In the presence of an alternating magnetic field, the domain walls move in a random fashion. When pinning imperfections intercept moving domain walls, the imperfections become decorated with immobile domain walls[6]. Figure 7 shows line imperfections which have been decorated by domain walls in an alternating magnetic field. These linear imperfections in the film are probably due to work damage in the substrate which was not completely removed in polishing.
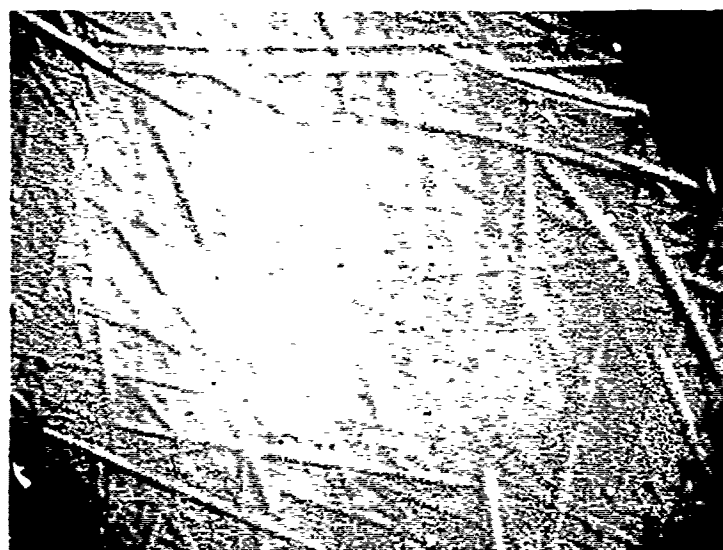
Figure 5.   Mechanical Damage in a Substrate Wafer Revealed by
Selective Chemical Etching (130X)

—| |—44 μm

Figure 6.   Domain Pattern of a Portion of GaYIG Film 2764Z3 on a DyGdGG Substrate
as Revealed by the Faraday Effect Under Zero Bias Field

—| |—44 μm

Figure 7.   Imperfections in the Same Portion of GaYIG Film 2764Z3
on a DyGdGG Substrate as Revealed by the Faraday Effect Under a
60 Hz Alternating Magnetic Field

13

2.1.2 Epitaxial Films

The unwanted generation or annihilation of bubble domains under a rotating magnetic field has been a major limitation to the utilization of GaYIG in bubble domain devices. This behavior is attributable to low wall energy which results from the high gallium content of GaYIG. (The gallium is required to lower the magnetization of YIG.) Since the wall energy is defined as $\sigma_w = 4\sqrt{AK_u}$ where A is the exchange constant and K_u is the uniaxial anisotropy, increasing K_u should raise σ_w.

GaYIG is deposited by chemical vapor deposition on DyGdGG substrates and the films rely on stress-induced anisotropy for bubble domain formation. The uniaxial anisotropy in a film may be increased by increasing the lattice parameter mismatch between film and substrate; however, the useful limit occurs just below the mismatch which causes a film to crack. A series of experiments were carried out with substrates of increasing lattice parameter in order to prepare films with the maximum amount of stress and hence increased values of wall energy. It was possible to increase σ_w from the range of 0.03 to 0.05 erg/cm^2 up to about 0.1 erg/cm^2 in uncracked films. Unfortunately, this value is only about a half the value of σ_w in other bubble domain materials. Further, since the mixed rare earth garnet substrates available contained many point defects, the films had many imperfections. Thus, despite the increase in wall energy in these GaYIG films, unwanted bubble domains were nucleated in rotating magnetic fields so that this attempt to make GaYIG useful for bubble domain devices has been unsuccessful.

In the utilization of bubble domain materials for military applications, an area of concern is the effect of temperature on a device. For this purpose, measurements were made of the runout and collapse fields on two GaYIG samples below room temperature. Over the temperature range studied, the collapse and runout data are linear functions of temperature as shown in Figure 8. There is a certain amount of scatter in the data which reflects the uncertainty in the measurements. A striking feature of the Figure is that the operating range of sample 3106Z3-20A is about half again as great as that of sample 2761Z3. The cause for this behavior is not clear. The characteristics of these two materials at room temperature are presented in Table III. Sample 2671Z3 has a higher magnetization, greater characteristic length and is under greater tensile stress as indicated by the higher wall energy. The major differing characteristic is that this sample is a thinner film which places it slightly below Thiele's optimum film thickness.

Table III. Characteristics of Two GaYIG Films

	2761Z3	3106Z3-20
$4\pi M$ (gauss)	100	85
ℓ(μm)	1.2	0.9
σ_w(erg/cm^2)	0.10	0.05
h(μm)	3.0	6.3
h/ℓ	2.5	7.0

14
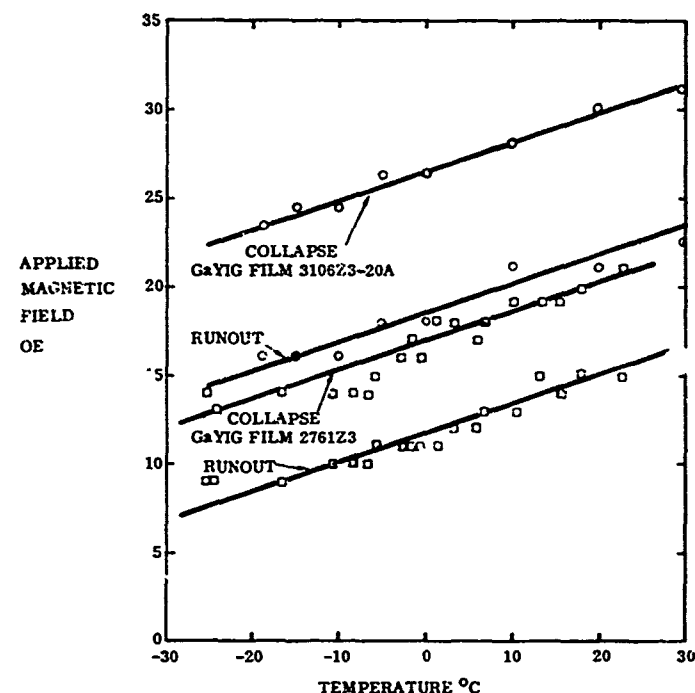
Figure 8. Runout and Collapse Fields of Two GaYIG
Films as a Function of Temperature

2.2 BUBBLE DOMAIN DEVICE DEVELOPMENT

Recent advances in the area of device physics and component design have been
made which contribute greatly to the basic understanding of device operation and to
the development of bubble domain memory systems. Since the operation of various
device components is highly dependent upon material properties it is difficult, if not
impossible, to separate material and device aspects without eliminating essential
features of the problem. For this reason and for completeness we have included the
following sections to review recent advances in the device area made in connection
with other programs in our laboratory. Of particular interest is the section on device
physics which appears as a completely new addition to the device summary presented
in the Annual Report.[1] The other sections on device components, device fabrication,
and peripheral electronics are updated versions of the earlier subject matter. Since
the emphasis of in-house programs is on the development of field access devices this
is reflected in the scope of the following review.

2.2.1 Advances in Device Physics

Up to this time the understanding of field access devices has largely been based
upon the following concept of operation: the uniform in-plane rotating field polarizes
the permalloy propagation pattern thereby creating localized poles which, if the
pattern is correctly designed, produce a field gradient at the bubble position causing
motion along a prescribed path.[7,8] Experimental evidence is overwhelmingly against
such an oversimplified picture and in fact, if the above interpretation were really
correct, it is unlikely that such devices would work. The fact is that the bubble field

15

plays a prominant role in the operation of the device. Both the bubble field and the drive field act to polarize the permalloy pattern the relative amount depending upon the magnetization of the garnet and the distance between the permalloy and the top of the bubble domain. The influence of the bubble may clearly be seen via bitter pattern observations.[7,9] Figure 9 shows such data for the case of a bubble at two different positions on a chevron track (see para 2.2.2.1). Comparing the domain patterns for adjacent chevrons (both with and without an applied field) illustrates the major role played by the bubble field. Further confirmation of the importance of the bubble field include (1) the observation that bubbles remain under the permalloy pattern during propagation, (2) the observation that bubbles grow in size when they move under a permalloy bar, and (3) the fact that a magnetoresistive detector actually works. Observations (1) and (2) are basically manifestations of the same effect. The bubble field just like the in-plane field polarizes the permalloy — the only difference being that the range of the bubble field[10,11,12] is only about a bubble radius. As a result when a bubble moves near a permalloy structure it polarizes that material and creates an energy well under it.[9,13] The result is that the bubble clings to the structure. The change in bubble radius which occurs when a bubble moves under the end of a bar is caused by the reduction in bias field due to the opposing field produced by the polarized bar and is confirmation of the energy well that exists under the structure. The magneto-resistive detector works because the bubble field is as effective in polarizing the detector element as the in-plane field with the result that the total in-plane field is out of phase with its rotating field counterpart, making differential detection possible.

The importance of the bubble field in device operation has also been confirmed theoretically. Figure 10 shows some calculated results[9,14] for an oversimplified structure — a simple bar. These results form the basis for understanding bubble propagation along more complicated patterns. The left half of the figure applies to bubble motion along the major bar axis while the right half applies to motion perpendicular to this axis. As was mentioned previously, since the bubble can lower its magnetostatic energy by moving under the bar, an energy well occurs there.

In Figure 10 this well appears below the bar as the symmetrical curve. As can be seen the energy of a bubble does not change appreciably until it is within a radius of the permalloy which is a reflection of the range of the bubble field. The occurrence of the two local minima near the ends of the bar is confirmed by the experimental observation that the center of a bubble normally does not sit at the end of a bar but rather, as the left-half of Figure 10 suggests, lies farther under the structure. The minima at the center of the bar changes to a local maximum for shorter bar lengths for motion along the major axis. Application of a uniform drive field collinear with the bar produces the asymmetrical solid curve in the left half of the figure, and depending upon orientation, the labelled solid curves in the right half of the figure. Experimental confirmation of this illustrated behavior has been obtained both for simple bars and for more realistic propagation structures.[15] The constant shift of these curves relative to the zero field curves results from the interaction of the uniform applied field with the corresponding "uniform" magnetization distribution. For motion along the major axis of the bar the field gradient is almost constant yielding an effective drive field quite different from that expected on the basis of the field from the bar alone. Neglecting the polarizing influence of the bubble field yields the dashed curve shown in the left half of the figure.
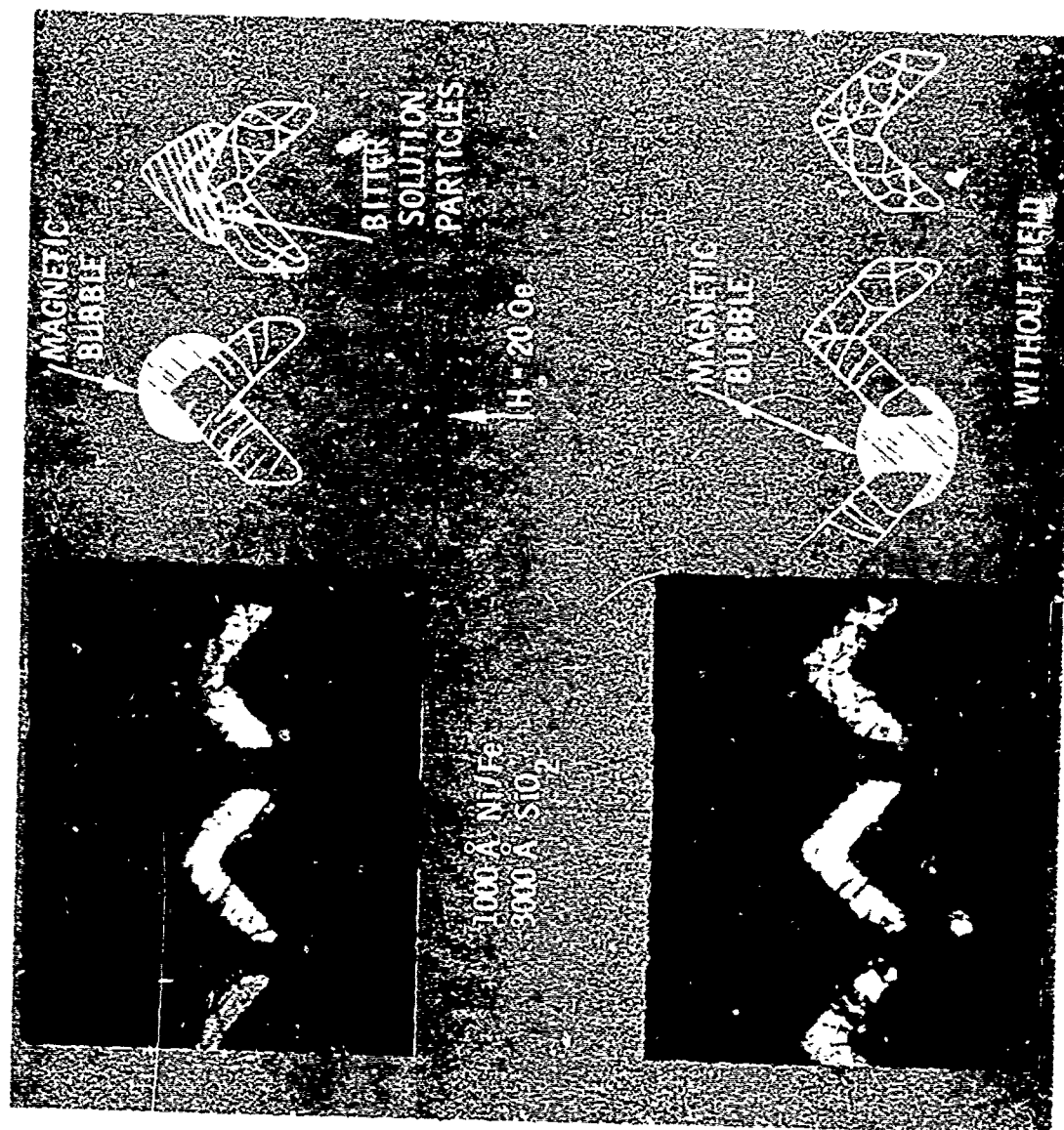
16

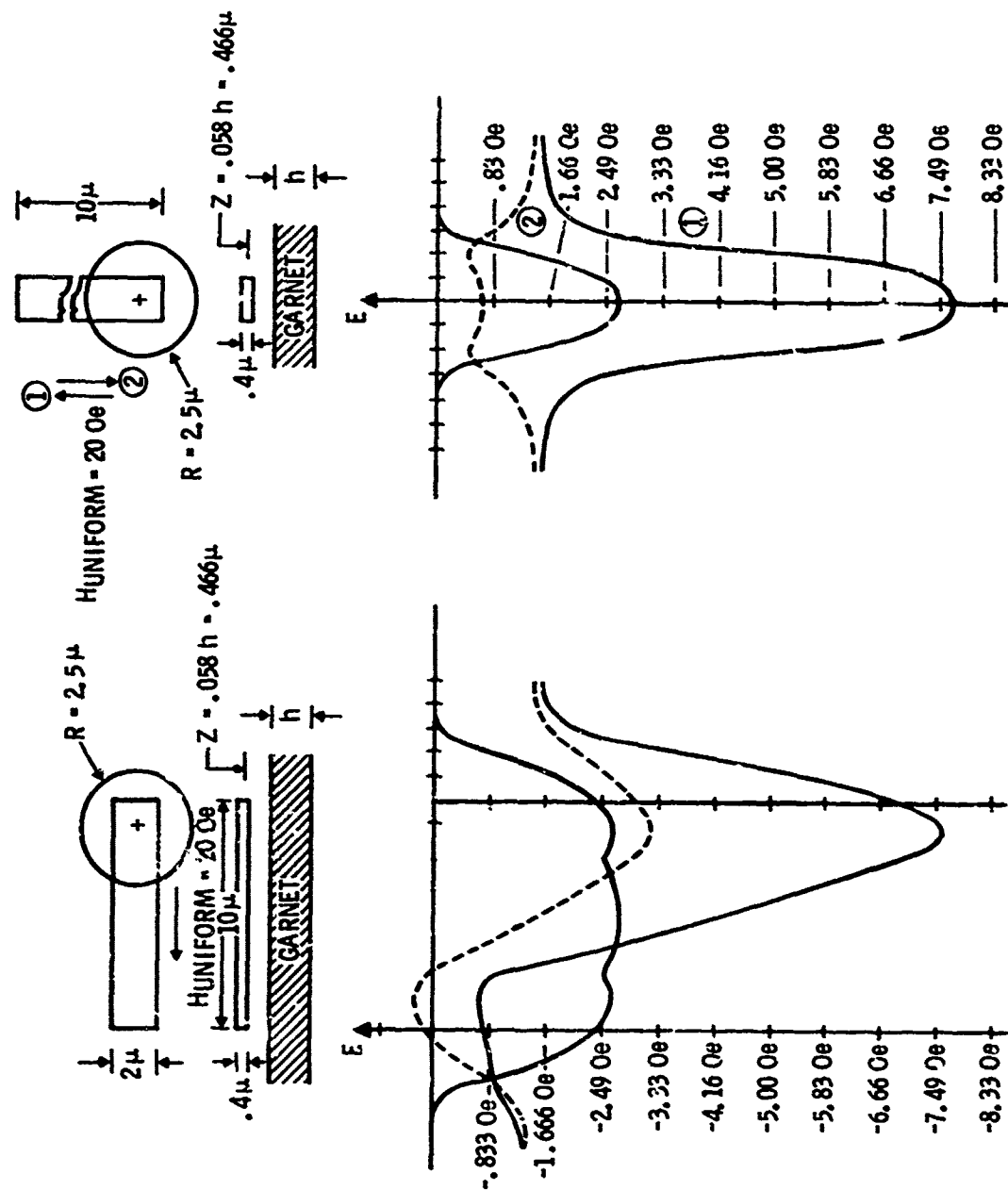Figure 9. Bitter Pattern Observations on a Chevron Propagation Pattern

Figure 10. The Calculated Potential Wells and Drive Fields for a Simple Bar

18

The calculation of the drive fields for a more realistic propagation structure is complicated by the interaction between adjacent permalloy bars. For a completely general treatment, it is necessary to take this interaction into account explicitly. When the spacing between elements is a linewidth or more, however, estimates indicate that to a first approximation the elements can be treated independently. Using the analysis for a simple bar, it has been possible to analyze the two-sided bar propagation circuit completely using this approximation. Figure 11 shows the results for two somewhat simpler configurations — Bar-Bar and I-Bar pairs.

In Figure 11 the application of a field in a particular direction causes a bubble to move from one bar to the other. If one compares the curves in Figure 11 with those for no applied field, it becomes clear that this motion is the result of motion of the energy minima from one point to another. Since the bubble is energetically tied to this minima, in a realistic propagation structure, the bubble is swept along the track by the moving energy minima. This is illustrated in Figure 12 for a two sided bar propagation pattern[16] for four positions of the rotating field. The location of the energy minima corresponding to the four field positions is indicated by the circled numbers at the bottom of the figure. Motion in this case proceeds from right to left and for 90 degree rotations of the field the spatial separation of the energy minima is quite non-uniform. This figure is the basis of current understanding of device operation and taken together with Figure 10 and the associate concepts gives one the necessary background to understand and improve existing device components.

2.2.2 Advances in Component Design

The basic building blocks required to realize a shift register memory[17] are: (1) a propagation track, (2) a generator, (3) a detector, (4) a switch, and (5) an annihilator. Early versions of the first three of these device components were discussed in the previous Annual Report.[1] A number of improvements in these components have been made following the appearance of that document which warrant explanation. While the advances in this area come rather hard due to the trial and error approach necessary to design these elements, a clear pattern of progress is beginning to emerge. Developments in this area of bubble-to-bubble logic[18,19] have come somewhat more slowly due for the most part to the rather small short range interaction between bubbles. Since work in the logic area is only in the preliminary stages and since the requirements for a bubble domain mass memory can be met using only the previously mentioned components, the emphasis of the following discussion will be placed on the five basic device building blocks.

2.2.2.1 Bubble Domain Propagation Track

A gradual evolution in what is thought to be the most desirable type of permalloy propagation pattern has recently been taking place. This evolution is traced from the T-bar through the chevron in Figure 13. Probably the most important step in this sequence is removal of the bar. Measurements of the potential well depth along the propagation path[15] indicate that by far the deepest well occurs under the bar. This is of course due to the fact that the bubble can easily polarize the bar parallel to its major axis. As a result, pulling-off the bar is relatively difficult and there-in lies the weak point of the circuit. Subsequent measurements comparing the margins of the Y-Y and T-bar structure tend to confirm this argument.[20] The operating margins
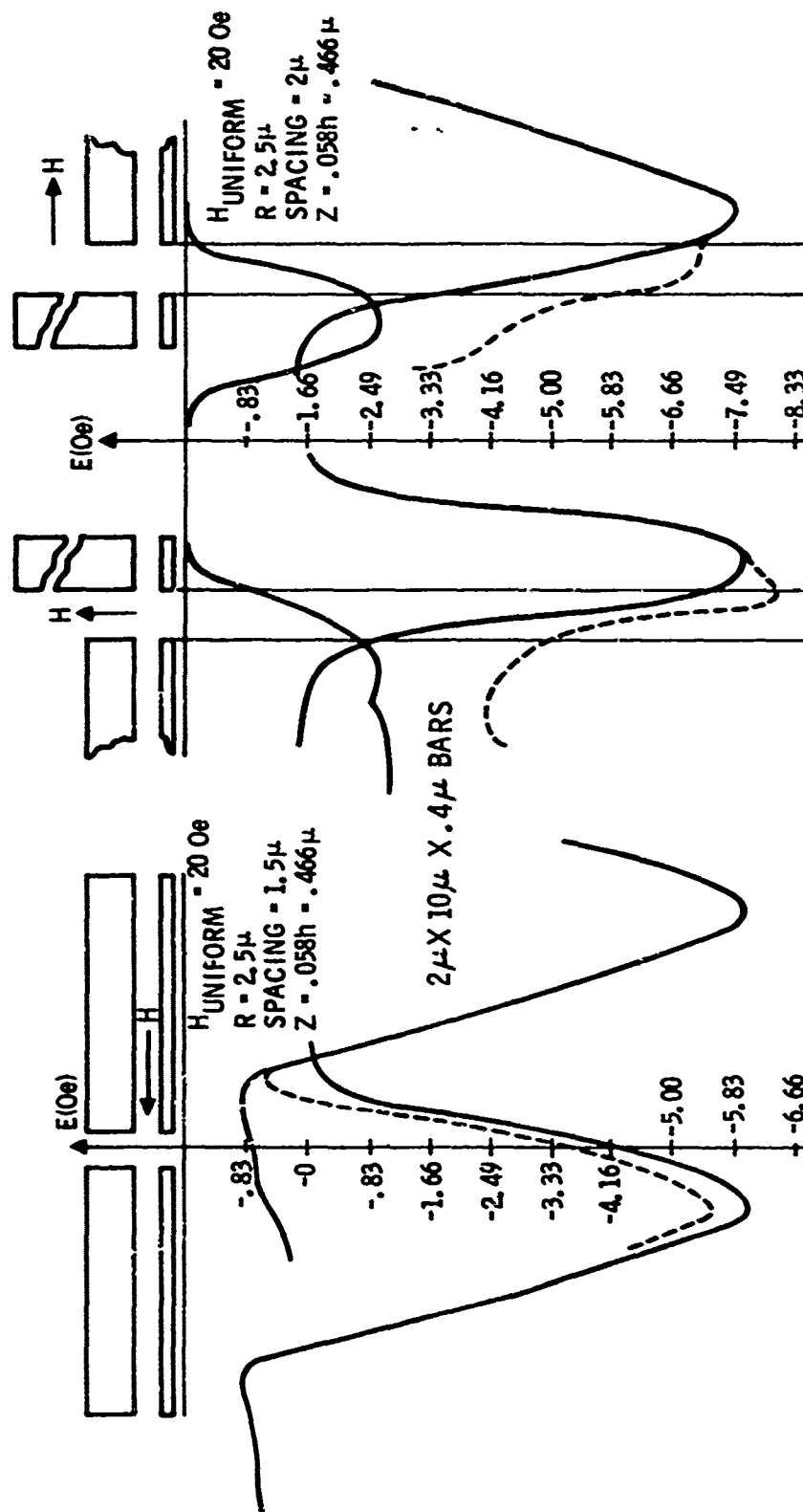
Figure 11. The Calculated Drive Fields for a Bar-Pair and an I-Bar Pair
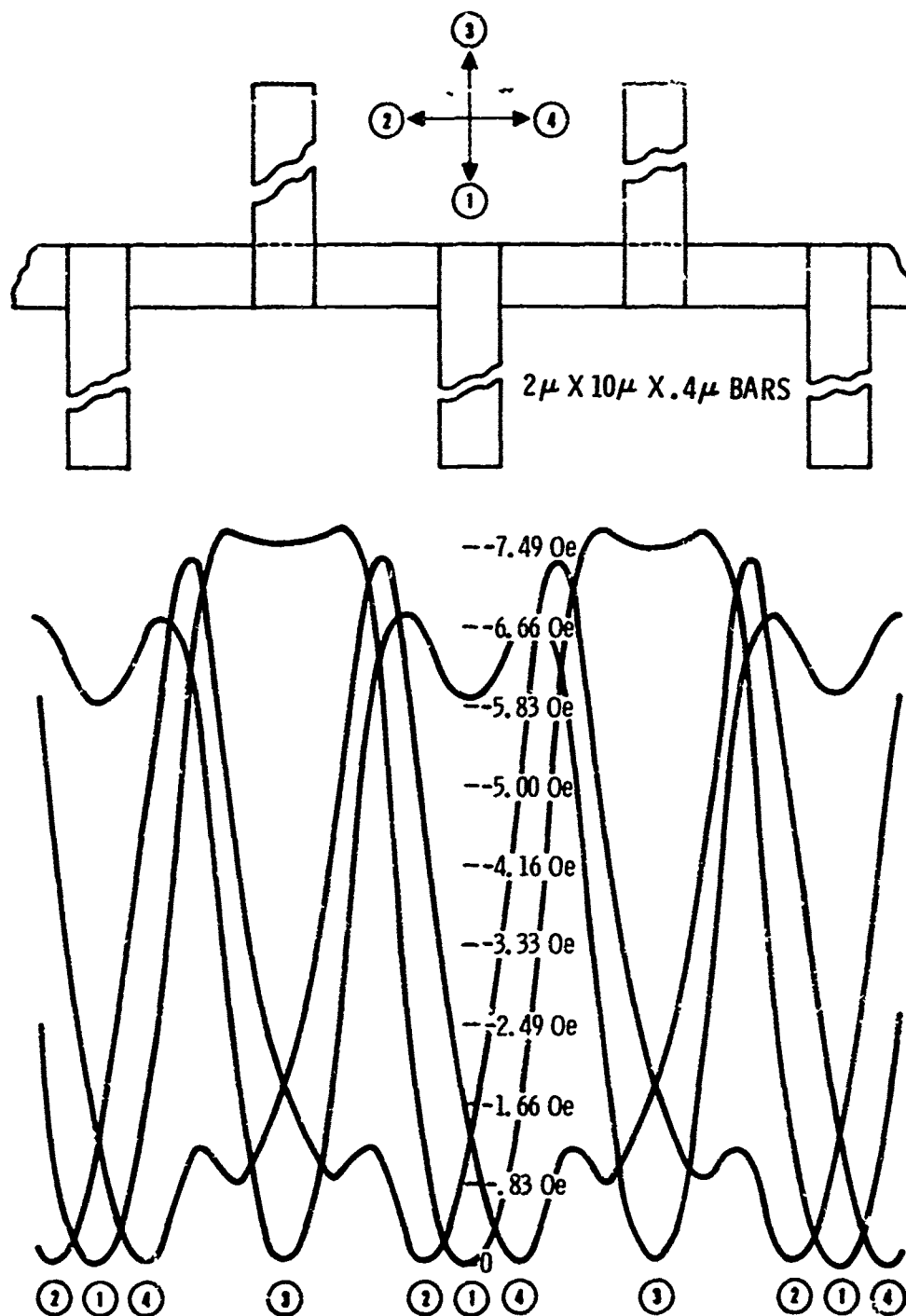
Figure 12.   The Calculated Drive Fields for a Two-Sided Bar
Propagation Pattern Showing Motion of the Energy Minima

21

T-BAR

Y-BAR

Y-Y

CHEVRON

MULTIPLE-BAR CHEVRON
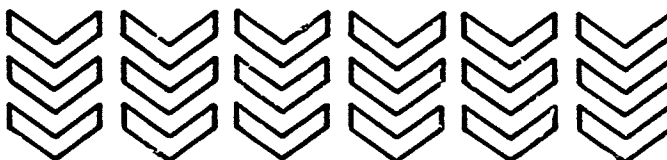
Figure 13.   The Evolution of Propagation Structures

22

for a Y-Y structure are appreciably larger than for a similar T-bar pattern. Surprisingly, removing the base of the Y seems to improve the operational characteristics of the Y-Y structure and leads to what is called the chevron pattern. [21] By removing the stub on the Y one would intuitively expect that the pole strength at this position would be decreased and hence the driving field at that point would also be decreased. Experimentally what one finds[15] for a chevron pattern is that the energy well depths in the presence or absence of an applied field are nearly the same at the equilibrium positions (bar ends and middle). This explains why the structure works so well — the drive fields are almost uniform along the track. Taken together with the equal spacing of the poles, this observation suggests that the chevron is probably the ultimate in propagation structures.

The multiple-bar chevron pattern[21] is an out-growth of attempts to construct bubble-bubble logic functions and may be regarded simply as a generalization of the chevron pattern. Both bubbles and strips can be propagated along this pattern with current interest being placed on the latter mode of operation. The multiple-bar chevron has some very desirable features when operated in this way. Foremost, is the fact that strips are easier to detect than bubbles because more field (not magnitude but area or volume) is available to switch a magnetoresistive element. Furthermore strips appear to be somewhat more immune to defects than bubbles. It has also been suggested that the effective drive field from a multiple-bar chevron is higher than that for a single bar device — whether this is indeed the case is yet to be confirmed. Figure 14 shows a typical margin curve taken on a three bar chevron on a low mobility sample. The data is for a simple racetrack which consists of both straight and curved sections of track. The rather narrow margin at 4 kHz is a consequence of the large gaps between permalloy elements which resulted from overetching.
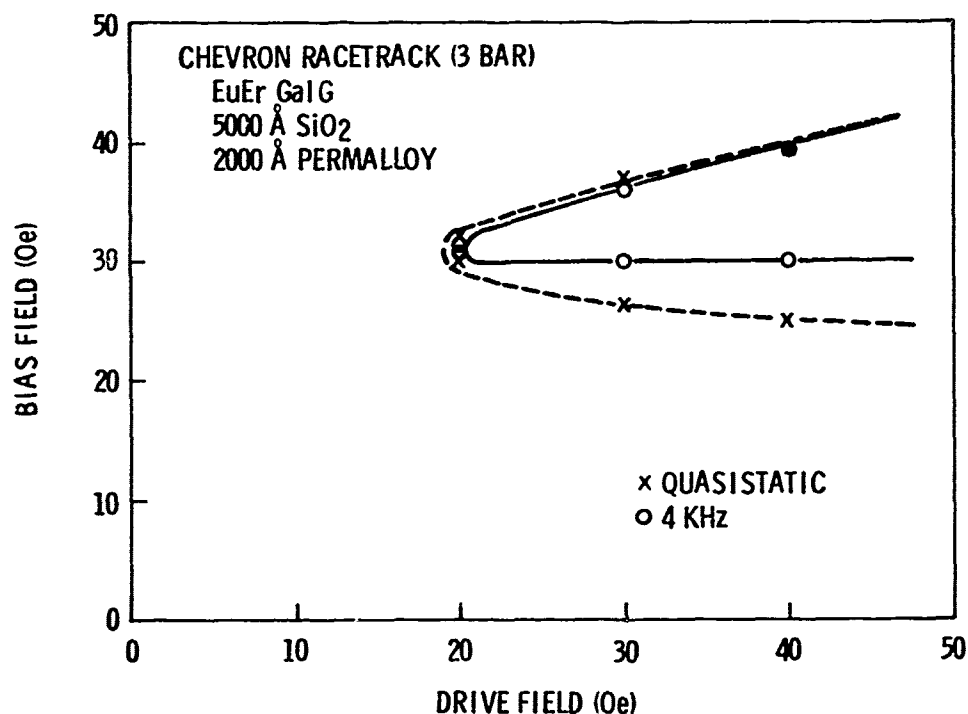
Figure 14. The Margins for a Three-Bar Chevron Racetrack

2.2.2.2 Generation and Annihilation of Bubble Domains

There are essentially two basic types of replication generators being considered for device applications — those that operate continuously[22, 23] and those that generate a bubble or strip upon command.[9, 21] Since the former, upon addition of a switch, can be substituted for the latter, the interest in both types is understandable. The keyhold generator which was one of the earliest types to be used in this laboratory has been successfully operated in the modified multiple-bar form[8] shown in Figure 15. The philosophy behind adding the additional bar is to extend the potential well further away from keyhole, thereby causing more strip-out and enabling a wide current conductor to be inserted as shown. The operation is very nearly the same as for the convention keyhole generator with the exception that the fabrication difficulties are somewhat reduced. The quasi-static margins shown in Figure 16 indicate that the device can successfully be operated over a range compatible with that of a typical propagation structure. One difficulty encountered with this generator is that for materials with a low wall energy (under some circumstances) it operates continuously. Since the margins for continuous and controlled propagation are generally wider than for controlled operation alone, it has been suggested that this generator be used continuously, employing a switch to shift the bubble to the desired path. Since switch margins are currently considerably narrower than that shown in Figure 16, it is doubtful whether this approach would be worthwhile. When and if switches become available with margins which approach that of the track, this technique may become more popular. It has the advantage that both functions may be optimized separately.

In the keyhole and other generators, the bubble generally circulates around a relatively large permalloy pad which produces a deep potential well locally, thus, binding the bubble to that vicinity. This is necessary in the keyhole design in order to produce stretching. If the pad is too small, or if the garnet to permalloy spacing is too large, it is possible that the seed bubble will enter the track making continued operation impossible. The well binding the seed to the permalloy can be produced in a variety of ways. Figure 17 shows how three bars can be used in this capacity. In this case, a strip oscillates back and forth between the bar ends under normal conditions. If a current pulse is applied to the cutting conductor, a portion of the strip is split-off and a bubble propagates out to the right. The device margins are shown on Figure 18 for this generator, and as can be seen, are considerably narrower than that for the associated Y-bar propagation pattern. The upward sloping low field generator margin reflects the tendency for the seed strip to strip-out as the drive field is increased. It has been suggested that similar designs with more bars[24] can be used to generate strips provided a multiple-bar chevron is arranged so as to "accept" the resulting domains. No report of the actual operation of such a device has yet been made, however.

Since the generation and annihilation functions are complementary and since they traditionally have been realized using the same basic permalloy pattern[1, 25] as that used for the generator, it is appropriate to include a section on annihilation here. Annihilation currently is accomplished by merging the bubble to be destroyed with one that is trapped under a permalloy pad. The operation is the inverse of continuous generation and its success depends upon the relative strengths of the bubble-permalloy and bubble-bubble interactions. So long as the former is larger than the latter, two bubbles under a pad will combine and the entering bubble will be annihilated. When the bubble-bubble interaction becomes too large, generally one bubble is kicked off the pad and the operation is unsuccessful. In the very simplest of terms, operating a generator backwards generally succeeds in annihilating bubbles.
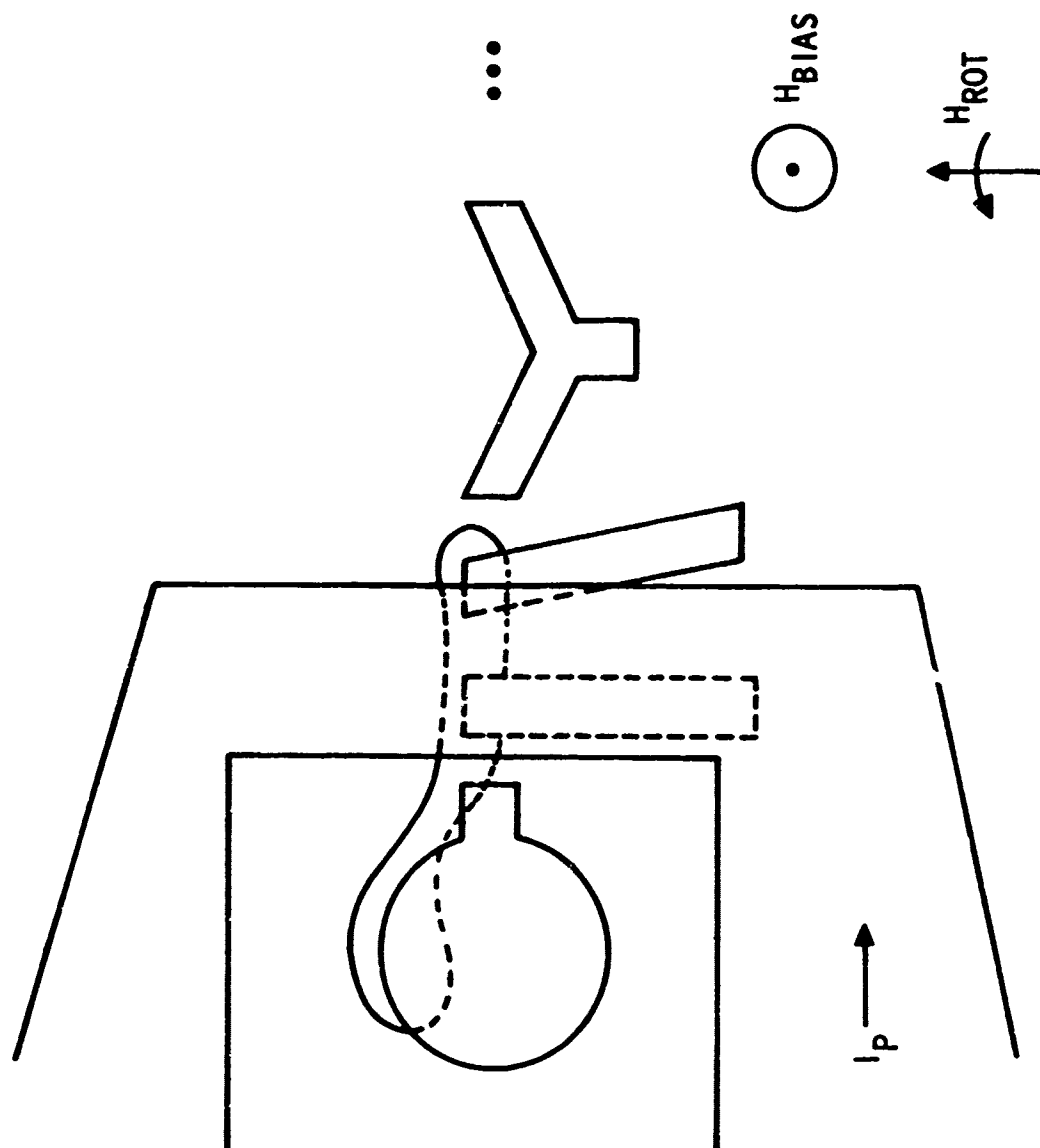
Figure 1b. The Multiple–Bar Keyhole Generator
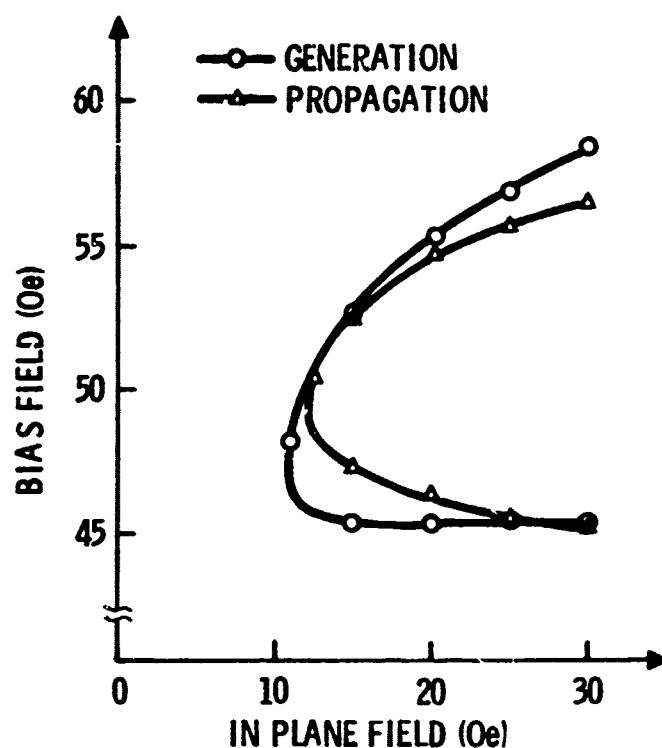
Figure 16. The Margins for a Multiple-Bar Keyhole Generator
and for a Chevron Propagation Track

Alternative techniques in which the bias field is locally raised to collapse the bubble by employing a current carrying conductor loop are now being investigated. The rapid spatial variation of the field as one moves away from the conductor makes the placement of the loop extremely critical — particularly in view of the fact that the currents required to increase the bias to the collapse field throughout the thickness of the garnet are prohibitively high. As of this time no strip annihilator of this type has been constructed, however, by simply bringing the strip down to a bubble by reducing the number of stacked chevrons spatially, a bubble annihilator may be employed.

2.2.2.3 Detection of Bubble Domains

The basis for using magnetoresistance to detect bubbles was discussed in the previous Annual Report.[1] The recent advances[4, 26] made in this area suggest that this type of detection is most likely to be chosen for device applications in the future. The problem in the past has been increasing the output in order to obtain usable signals. Once it was recognized that by stretching the bubble into a strip and allowing this domain to interact with the magnetoresistive element a larger output could be obtained, advances in detector design came rapidly. Figure 19 shows one of the first stretcher type detectors[26] operated successfully in this laboratory — the so called Chinese character detector named after the form the propagation pattern and magnetoresistive element take in the vicinity of the detector. In Figure 19 two broad gold leads which appear sandy in the photograph are connected to a thin permalloy detector bar (gray) which is constructed so as to reduce the transverse demagnetizing factor. The ends
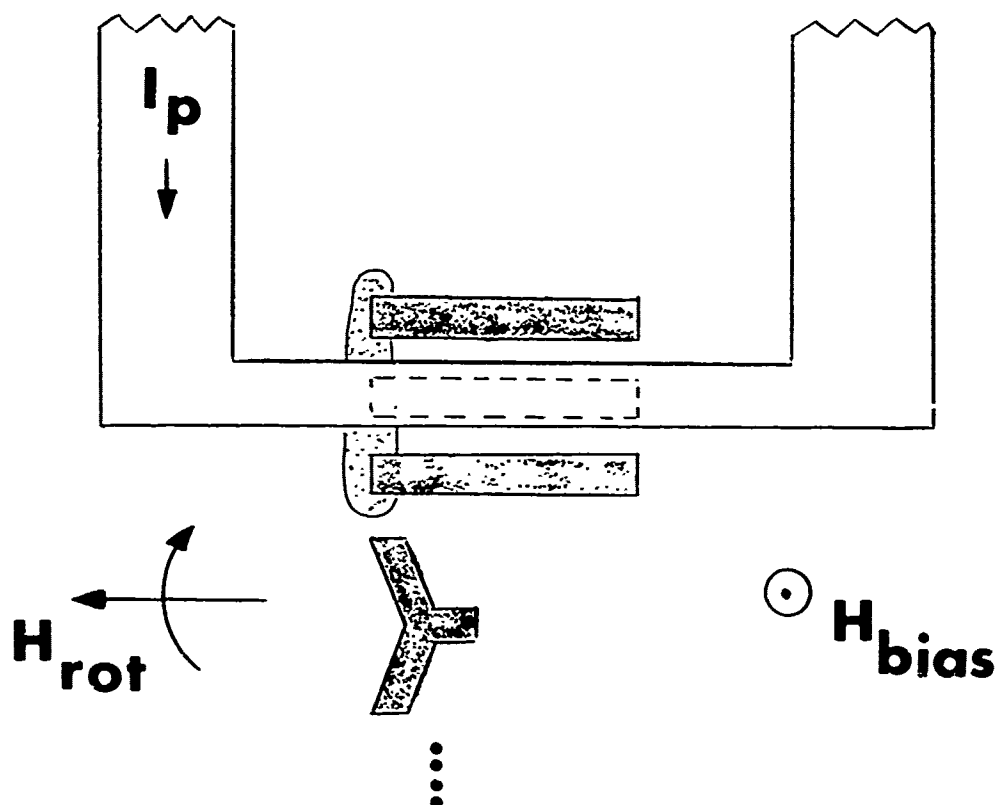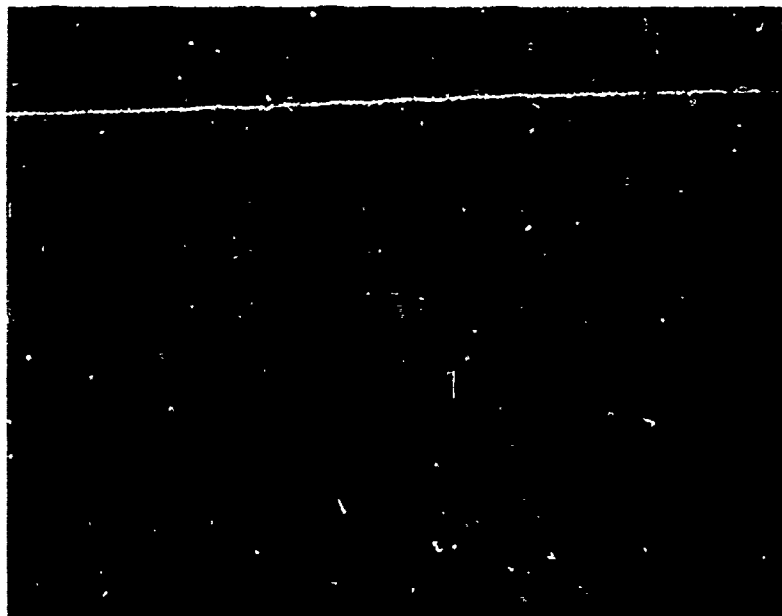
Figure 17. The Multiple-Bar-Strip-Type Generator Used for Generating Bubbles

27
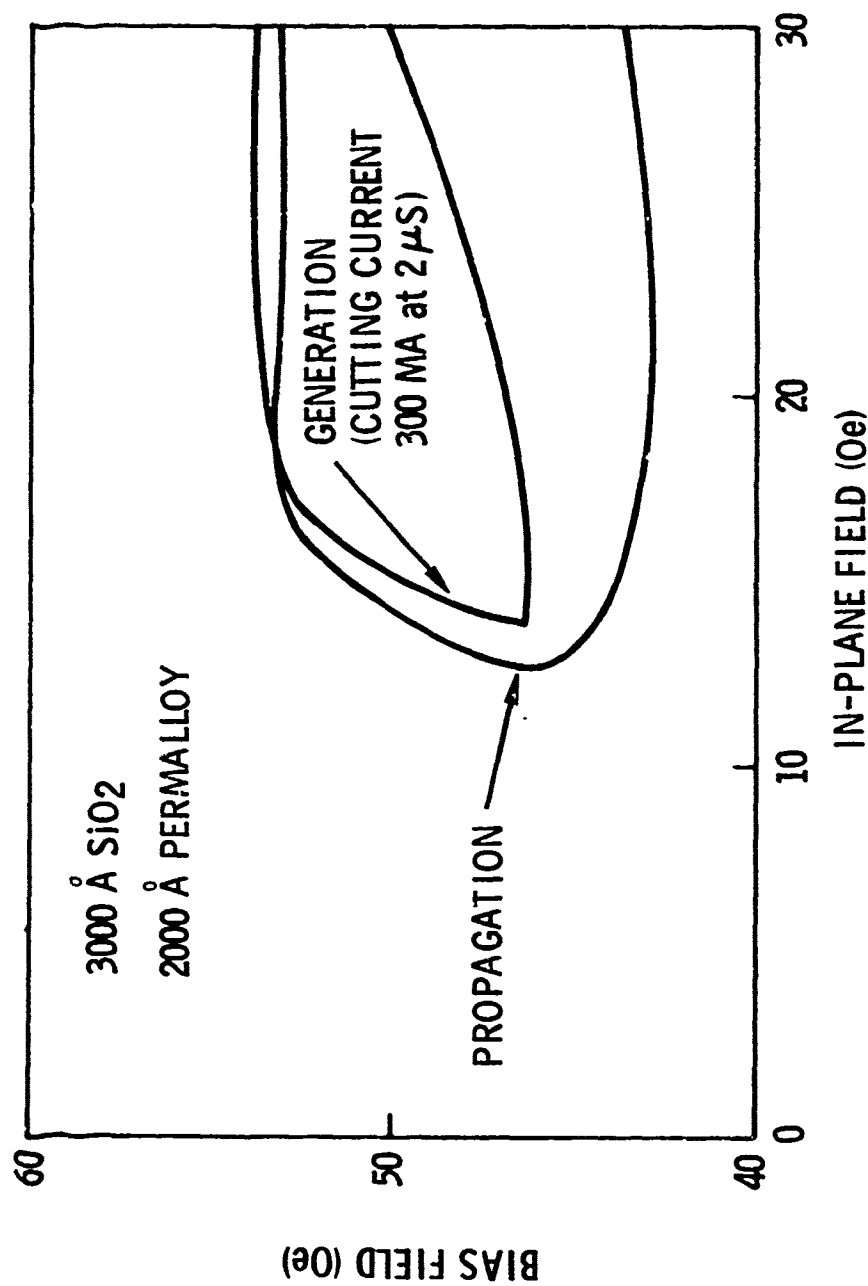
Figure 18. The Margins for Multiple-Bar-Strip-Type Generator and Y-Bar Propagation Structure

28
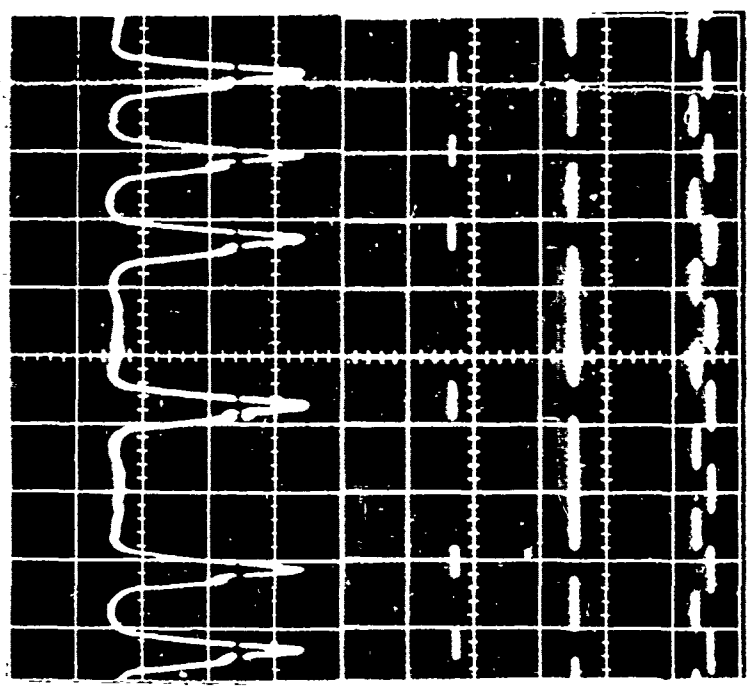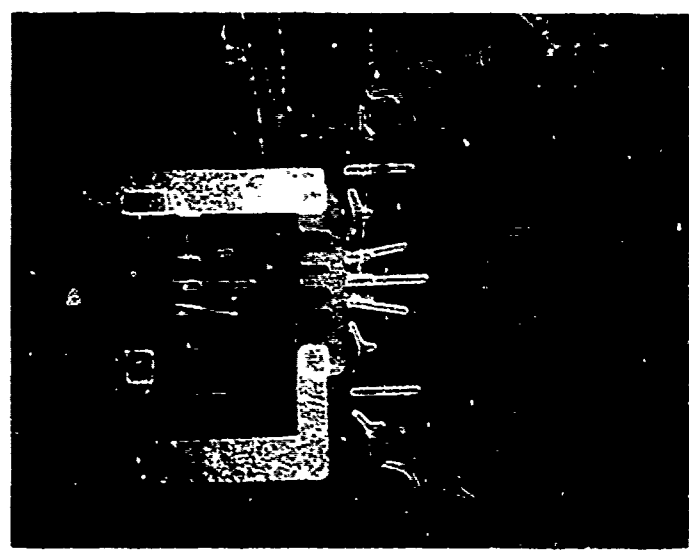
Figure 19. The Chinese Character Detector and Device Output
After Amplification and Signal Processing

of the "cross tie" bars of the thin element lie under the ends of a bubble stretcher in the propagation path. The bubble, as it moves by the thin element, stretches out into a strip and the bubble field polarizes the detector element nearly at a right angle to the rotating field direction with the result that a differential output between the actual detector and the dummy detector (immediately above) can be obtained. This output is shown to the right in Figure 19 for an 8 bit word. The quasi-static margin for the Chinese character detector shown in Figure 20 indicates that there is some degradation of propagation along the track. This is not unexpected in view of the stretching involved. At high frequencies one would expect this type of detector to falter due to the added velocity required for the strip to move the detector length in the allotted cycle. Accordingly, it seems reasonable that stretching perpendicular to the direction of motion of the bubble should bring an improvement in device operation. Figure 21 shows what probably will be regarded as the ultimate technique for bubble detection. The principle of operation is identical with that of the Chinese character detector. However, a much higher operational frequency is expected. The device shown in Figure 21 is designed for bubble detection, however, by adding chevron elements, strips will propagate through the detector which gives it added versatility. Figure 22 shows a photograph of a device of this type which was the first to be operated in our laboratory at low and modest frequencies. At intermediate frequencies, the limiting factor in this case was not the detector but in fact the propagation track. Work is now in progress to determine the optimum location of the thin detecting element. One difficulty connected with this device is that the thin permalloy bar tends to become discontinuous where it crosses a thick permalloy step, resulting in an "open" in certain designs. Care must be taken in the processing sequence so as to eliminate thermal shock which is assumed to cause the problem.
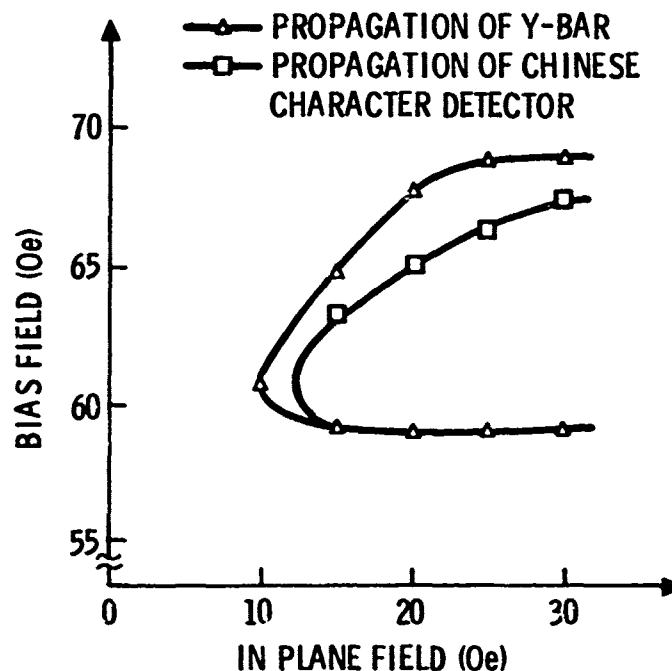
Figure 20. The Margins for a Chinese Character Detector
Operating in a Y-Bar Propagation Pattern

CHEVRON STRETCHER DETECTOR

2000 Å Permalloy

200 Å Permalloy

3000 Å Gold
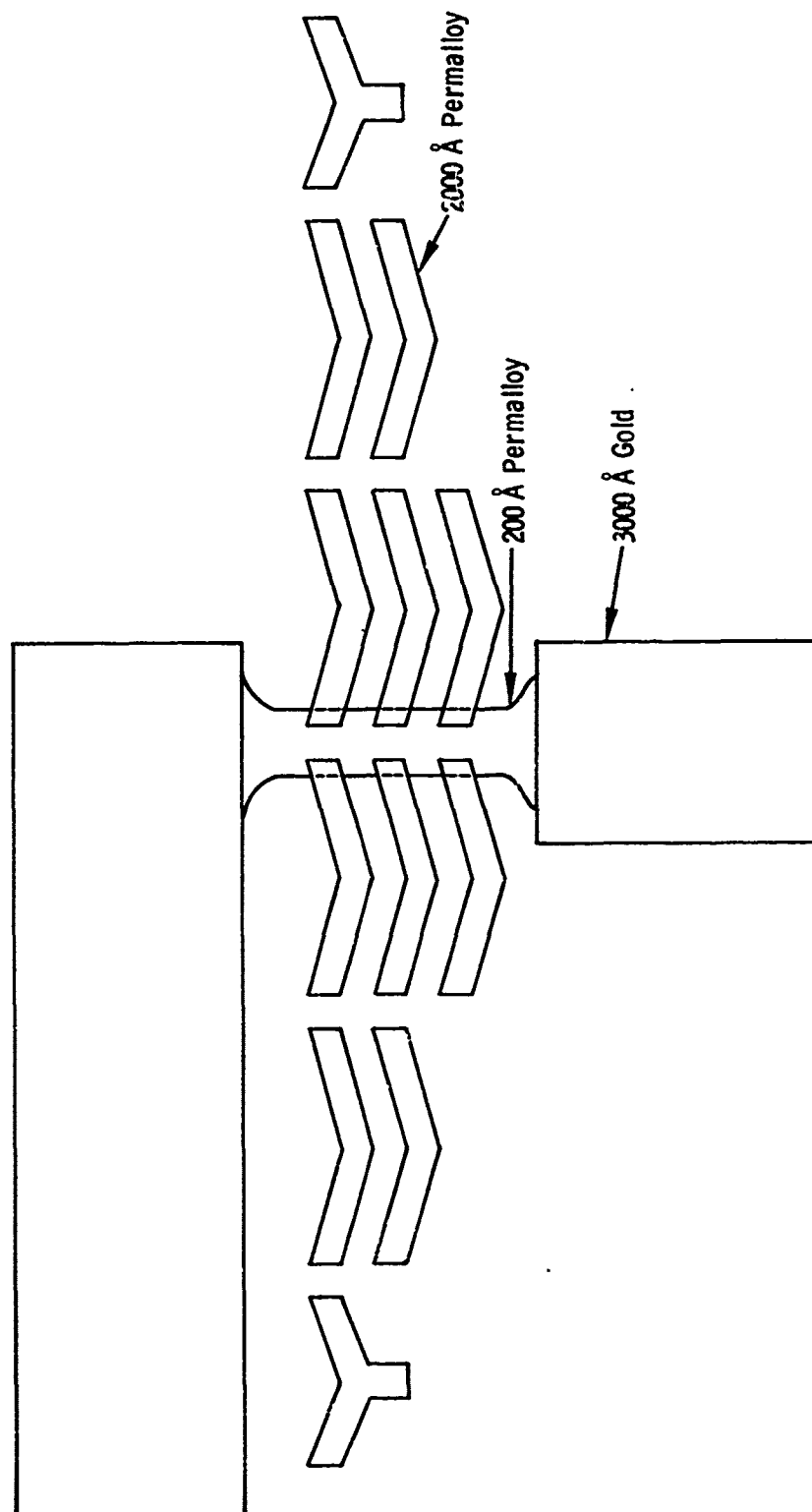
Figure 21. The Chevron Stretcher Detector

31
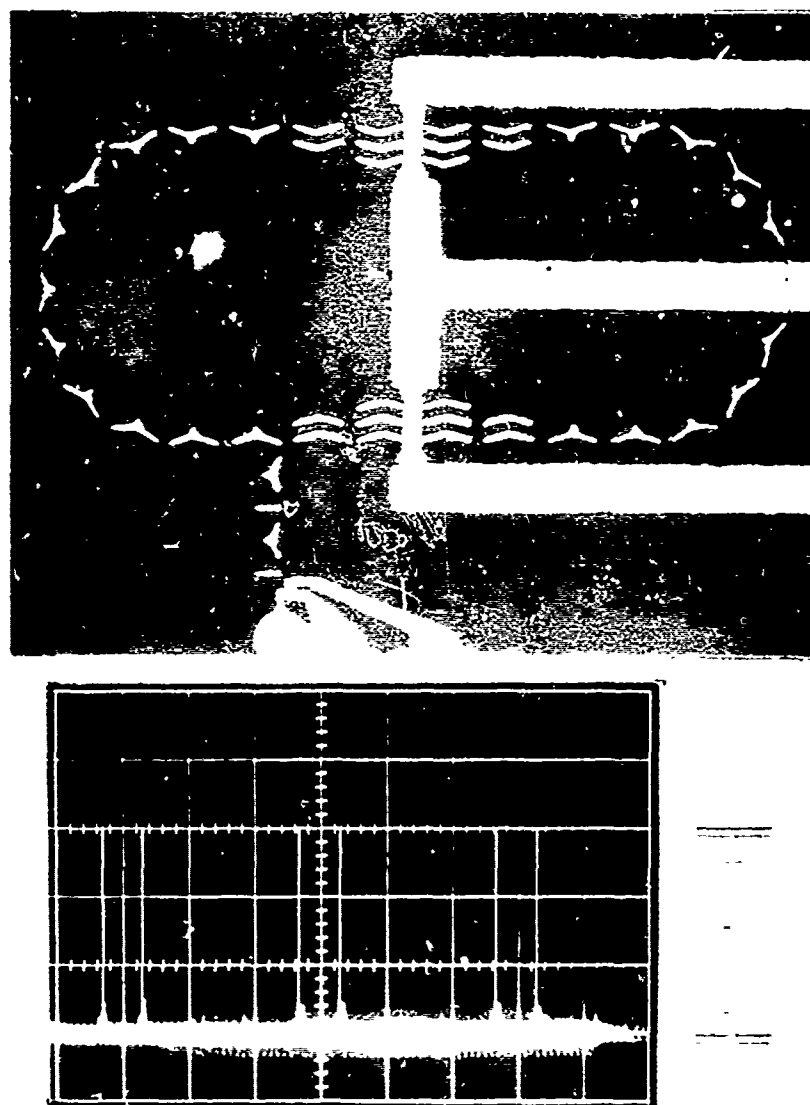
Figure 22. The Output From a Chevron Stretched Detector After Amplification

2.2.2.4 Current Controlled Logic-Bubble Domain Switching

A switch is essential to the construction of a shift register bubble memory as it is currently the only way information can be removed from the storage loop. It would also be extremely convenient to be able to access any one of a number of different storage loops on a chip by employing a bubble decoder. A branch or tree decoder of this type can be constructed provided a reliable current controlled switch can be realized.[25] The major-minor loop form of system organization[27] requires that information be switched into and out of a minor storage loop — a more difficult task than just switching out of a closed loop. The bubble domain switch at this time remains the most difficult function to realize as is confirmed by the observation that overall device margins invariably are determined by this component. Figure 23 shows a current controlled switch which is now being used in a 64-bit bubble shift register (BSR) to switch bubbles from the storage loop into the annihilator. While fairly reliable operation of this component has been obtained, it suffers from a rather low margin (≥ 4 to 5 OE). The operation of this switch is based upon pulling the bubble away from the main track and onto the short section leading to the annihilator, which in this case is simply a bar. This is accomplished by activating the current conductor, thereby producing a field gradient perpendicular to the normal propagation path and drawing the bubble to the right angled permalloy element. Alignment of the gold conductor relative to the permalloy pattern is fairly critical because the gradient changes sign if the spacing between the main track and the conductor is too great. This switch operates only when current flows in the conductor — the bubble continues along a straight path otherwise. Other switches have been proposed and constructed in which
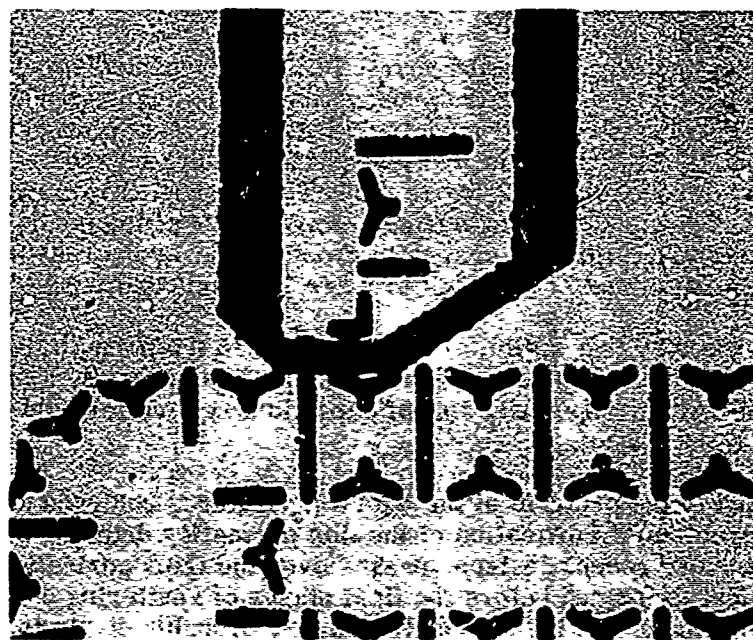
Figure 23. The Current Controlled Annihilator Switch Being Used on a
64 Bit Bubble Shift Register

33

a change in the current direction produces the switching action. [23] The disadvantage with the latter approach is that a constant current must flow through the device which is inconvenient from the supply stand-point (volatility). Furthermore, the margins for these components are no better than for the switch show in Figure 23.

A number of other switches have been proposed and in some cases have been operated. Of particular interest is the dollar sign switch[22] recently announced by Bell Telephone Laboratories to be used for major-minor loop transfer. For six micron bubbles, it appears that the fabrication of this device will require rather sophisticated technology. In view of the lack of experimental data it is impossible at this time to judge whether this particular device component will make an impact on the development of current controlled switches. Unlike the bias modulation switch[20] which appears to be a novelty more than anything else, the dollar sign switch has the possibility of becoming quite important if the claims of wide device margins are indeed realizable.

2.2.2.5 Advances in Device Fabrication

As device improvements have been made, it has been necessary to modify the processing sequence used in the past. It was realized quite early that the overlay technique has some disadvantages in terms of operational reproducibility. While this problem is not as severe as was first expected, fabrication of bubble domain devices directly on garnet substrates (as is now commonly done) has yielded some important dividends. Using an SiO_2 spacer between the garnet and propagation permalloy, which is sputtered directly on the SiO_2, has allowed important studies of the spacing dependence of the margins to be made. [9] Reproducibility of quasi-static margins has been obtained to within a few oersteds using this fabrication technique. Furthermore, to the degree that the SiO_2 thickness is known (± 250Å), one knows the spacing — which yields accuracies not available using the overlay technique.

Going to fabrication directly on the garnet initially presented some problems which were quickly overcome. Since the propagation permalloy goes down first in this process sequence, there was some degradation of its properties when gold was sputtered over to form the leads. This problem was traced to the elevated substrate temperatures which were obtained during gold deposition. When the deposition rate exceeds 400Å/min (300-400 watts rf power), the high surface temperature promotes gold diffusion into the permalloy, thereby degrading its magnetic properties. By decreasing the gold deposition rate to 240Å/min or below, this problem is eliminated.

It has been suggested that a similar improvement in the permalloy properties can be obtained by E-beam evaporation of the gold which is generally a milder process than sputtering. As earlier reported, 50Å of chromium is used for gold adhesion to the SiO_2 layer.

Closely related to the problem of the high temperatures achieved during gold sputtering, is the problem of fabrication of the thin permalloy detector bar (200Å in Figure 22) which in more recent designs, passes over the thick permalloy propagation track. If this element is formed before the final stages of sputtering chromium and gold, it invariably opens at the thick permalloy steps, probably due to thermal shock.

34

The result is that in designs where the detector element completely overlaps the chevron bars (as opposed to being between then as shown in Figure 22), the circuit cannot be used. The simplest solution to this problem appears to be to leave the fabrication of the thin detector element to last. The process sequence now being used to fabricate complete devices on garnet using standard photolithography is shown in Figure 24. Some variation in technique is obviously possible and may be desirable for higher outputs — the difficulty in doing this remains the degradation of its magnetic properties. A buried detector bar approach has been suggested, however, it would probably involve covering the permalloy with sputtered SiO_2, which would very likely be detrimental.
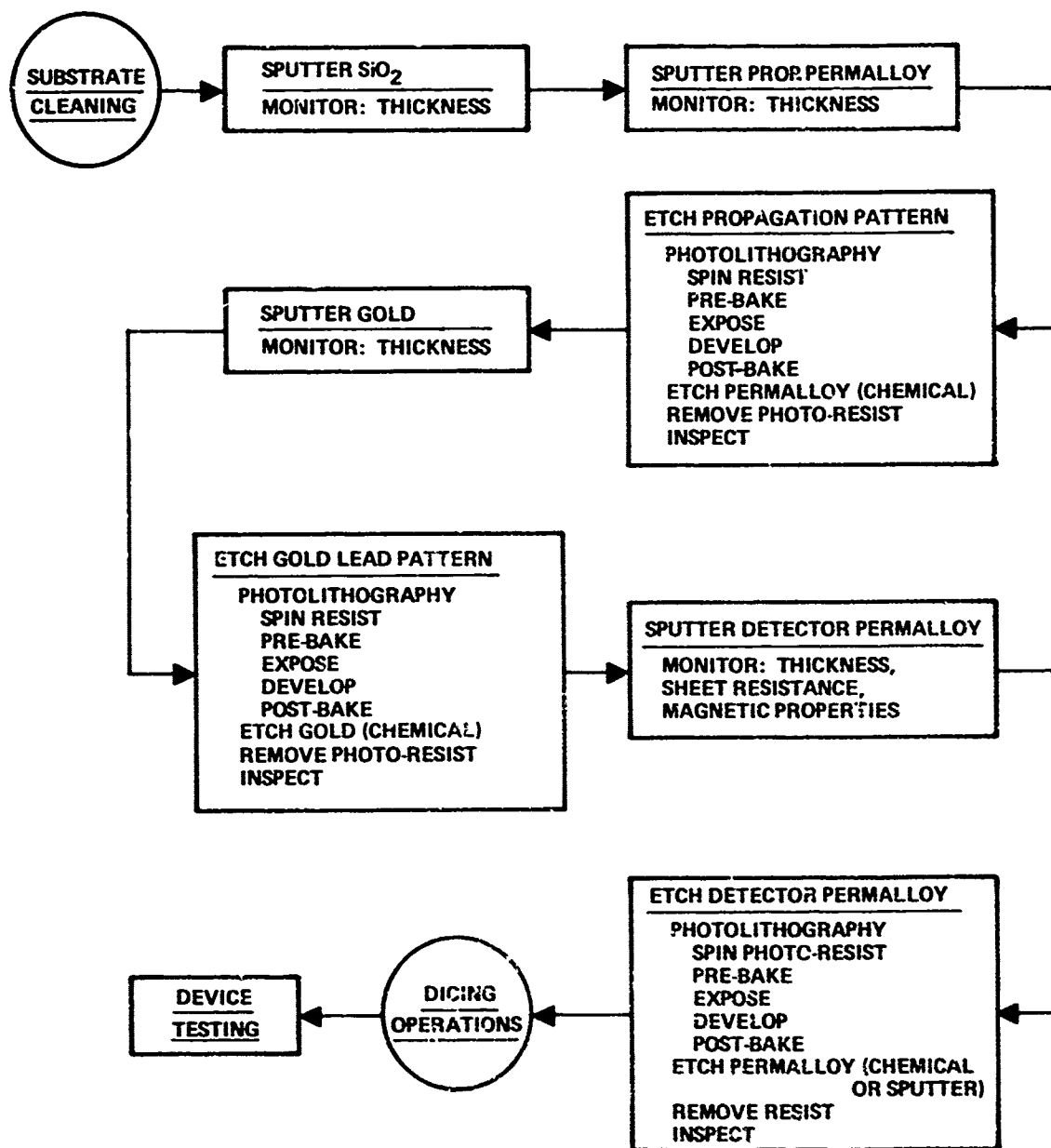
Figure 24. The Device Fabrication Process Sequence

35

2.3 ADVANCES IN PERIPHERAL ELECTRONICS AND HARDWARE

During the past 6-month period, bubble domain memory devices and associated magnetic field producing hardware and electronics have been advanced from a shift register with (1) low speed, visual only (no electronic) readout, (2) manual control of generator and annihilator pulses, and (3) a rack of electronic control equipment to a shift register with (1) 15 kHz addressed readout of four and eight-bit data words, (2) automatic control of generator and annihilator pulses to provide 15 kHz addressed entry of four and eight-bit data words, and (3) a 5.25 inch high rack-mounted electronic control unit.

2.3.1 Overlay Circuit Boards

The overlay mounting structures used 6 months ago consisted of 4 x 1 x 1/16 inch double-sided printed circuit boards with preamplifier circuitry mounted on an overlay glass in the center. For iron core rotating field coil operation, a glass tube pedestal was used on the circuit board to elevate the overlay to the center of the rotating field coil assembly. Use of the overlay glass to mount the preamplifier circuitry complicated the overlay fabrication; therefore, the preamplifier circuitry has been moved to the circuit board with considerable overall simplification. The recently fabricated circuit boards are reduced in width to 0.475 and 0.375 inch for 1.75 and 1.00-inch octagonal coils, respectively, and troughs have been milled out in the center of the circuit boards to allow easy mounting of overlays.

2.3.2 Rotating Field Coil Assemblies

The iron core coil assemblies used 6 months ago were limited to operation below roughly 1 kHz and the phenolic core coil assemblies were limited to roughly 10 kHz and operated at an undesirably high temperature. To achieve higher frequency operation with reasonably low cost electronic amplifiers and to achieve cool operation of the rotating field coil assembly, the physical size of the coil assembly was reduced considerably making it possible to obtain the required field magnitude using less ampere turns. To allow reduction of the coil assembly size, the circuit board assembly was made to insert into the coil assembly diagonally and the circuit board width was reduced. A 1.75-inch octagonal-shaped coil assembly was designed in conjunction with a 0.475-inch wide overlay circuit board, and a 1.00-inch octagonal-shaped coil assembly was designed in conjunction with a 0.375-inch wide circuit board. These coil assemblies were wound with and without viewing holes, for microscope observation of domain behavior, and were wound with several sizes of wire for optimum operation in several frequency bands. Smaller circuit board connectors were used and the connectors are being mounted on the coil assembly. Some of the coil assemblies have been operated at up to 1 MHz at fields ($\approx$30 Oe) which will cause propagation in typical bubble domain materials.

2.3.3 Bias Field Assemblies

Both electromagnet and permanent magnet bias field assemblies have been used with good success. The electromagnet bias field assemblies are the same design as that used for the original phenolic core rotating field coil assemblies. The permanent magnet bias field assemblies consist of square sheet-iron pole pieces with cylindrical permanent magnets between the pole pieces in the corners. Manual adjustment of the field strength is achieved by rotation of lead screws which move the magnets in-and-out.

Movement of the magnets out from between the pole pieces reduces the field strength by reducing the cross-sectional area of the magnetic flux path.

2.3.4 Electronics

The electronic control equipment used 6 months ago to generate voltage and current waveforms for the magnetic field generating coils, overlay current loops, and overlay detector circuits consisted basically of a waveform generator, separate power supplies, a pulse generator, a two-phase generator, and another unit for generating waveforms for gated propagation. Now, all these units have been integrated into one small unit, and addressed entry, addressed readout, and error detection circuitry have been added.

2.3.4.1 Rotating Drive Field Coil Amplifier

Two types of rotating drive field coil amplifiers were in use 6 months ago. One, used for linear amplification of voltage waveforms from a sine-cosine potentiometer or two-phase sine wave generator, consisted of an integrated circuit operational amplifier followed by an integrated circuit power booster followed by a complementary power transistor emitter-follower. This combination provided about ± 10 volts at about ± 3 amperes. The other amplifier type consisted of a nonlinear on-off power transistor amplifier that fed square waves to a resonant circuit.

Now, a high-voltage high-slew-rate power hybrid operational amplifier is used with paralleled complementary power transistor emitter-followers to provide up to ± 37.5 volts at ± 20 amperes or more, depending upon how many complementary emitter-followers are paralleled. The need for both a high voltage and a high current capability from the amplifiers may seem to imply that high power is needed, but this is not true, because both high voltage and high current are needed only at high frequencies where the power factor is small. This amplifier is used for both gated and continuous operation of the drive field.

2.3.4.2 Propagation Gate Generator

Initial gated propagation experiments were conducted at low frequencies using digital (on-off) drive waveforms or sine waves gated with FET's before linear amplification. These experiments were successful, but at higher frequencies it was necessary to use series resonant circuits to obtain the necessary high voltages, since transistors will not switch voltages as high (up to 1000v) as are sometimes needed for the coils used. The series resonant circuits have the disadvantage that a number of cycles are required for the resonant circuit voltage to build up to the necessary value. Although a capacitor can be used to store energy to start the resonant circuit at full amplitude within one-quarter cycle, there still is the problem of a high voltage switching transistor. Series resonant circuits are also inconvenient because they have to be tuned as the operating frequency is changed. It appears, therefore, that for non-gated propagation applications, series resonant drive coil techniques are good because drive amplifiers can be simple, low-voltage, efficient switching types but for gated propagation applications, the series resonant drive coil technique is not as simple as other techniques.

Ths use of small coils and high-voltage, high-current amplifiers allows gated propagation techniques to be used without using series resonant circuits. To start and

stop the drive field without altering memory information, the current in one drive coil (x-coil for example) should be allowed to build up, then both coil currents should vary sinusoidally and 90 deg apart until stop time when the x-coil current should continue one quarter cycle after the y-coil current is stopped. The propagation gate generator used to control these current waveforms derives a clock signal from the reference two-phase generator which is four times the frequency of the two-phase generator. This allows digital logic circuitry to select the appropriate one of four sine wave zero-crossings for sine wave gating. Delays, which are a function of frequency, are introduced which cause waveforms to switch as the currents go through zero.

2.3.4.3 Detector Circuitry

The preamplifier circuitry being used is essentially the same as that being used 6 months ago before good detector operation was achieved. The preamplifier differential outputs are AC-coupled into a differential input level detector, and the single-ended output of the level detector is used as the direct set input to a flip-flop. The direct set input is used instead of the clocked set input so the detector output can be allowed to occur anywhere between clock pulses, and the clock pulse always resets the flip-flop when the detector output sets it. This causes the detector flip-flop to be synchronous with the clock pulse and allows it to be used to drive any logical component, in a synchronous system using the same clock pulse, with correct timing.

Cancelling of $d\phi/dt$ pickup in the detector circuits due to the rotating field has been done successfully by summing with the detector voltage a drive field voltage of opposite phase and equal amplitude with that of the induced voltage. Use of printed circuitry in the plane of the rotating field with very short interconnecting bonded gold wires between the detector and preamplifier has resulted in $d\phi/dt$ pickup so small that no cancelling is needed at frequencies up to roughly 20 kHz.

At higher operating frequencies, if cancelling of the $d\phi/dt$ pickup does not provide adequate reduction of unwanted signals, then notch filtering and bandpass filtering will be tried. Then, if necessary, r-f excited detectors with high pass filtering and synchronous demodulation will be tried.

2.3.4.4 Exerciser Circuitry

After development of the magnetoresistive bridge bubble domain detector to achieve usable output, the digital logic circuitry and associated input output devices were assembled to allow easy determination of the bubble domain memory performance. A field rotation counter (memory timing or fast address counter) is necessary to synchronize the oscilloscope for observation of detected circulating bubble domains. This counter can be inhibited at each entry or readout of data to cause sequential entry or readout of data, but a second counter of equal period (slow address counter) is necessary to achieve addressed entry and readout of data. These counters were mechanized in each of three memory exercisers. The first exerciser used eight-bit words, thumbwheel switch programmable memory size, thumbwheel switch address preset, decimal address display, address increment up or down at entry, and readout and automatic comparison of stored and input data. It was used in conjunction with the waveform generator. The second exerciser was similar to the first except it combined the waveform generator and exerciser, had four frequency bands, automatic phase delay with frequency for generator and annihilator pulse generators, and had additional pulse generators for testing major-minor loops.

38

The third exerciser which is under development is basically a 16-word x 4-bit simplification of the second. Interconnections between the exerciser and memory module are made using exerciser panel banana jacks for x-y coil wires, bnc jacks for preamplifier output and an MS type connector for other connections. BNC jacks are used for monitoring x-y coil voltages and currents as well as for monitoring the annihilator and splitter pulses. A panel x-y gain control controls x and y gain together with the x-y gain ratio being controlled by a chassis-mounted potentiometer. Coarse and fine frequency controls permit selection of operating frequencies in two ranges. The memory address is displayed as a 4-bit binary number. Each time the Enter pushbutton is depressed, the input switch data is entered into the bubble memory at the indicated address and the memory address is incremented-ready for entry of a new word. Each time the Read pushbutton is depressed, memory information at the indicated address is read and displayed on the Data Out lights. The Continuous Read switch allows each four bit word stored in the memory to be displayed sequentially as the memory information circulates. The Address Reset pushbutton allows the memory address to be reset to zero. The Error light comes on any time a word read from the memory does not agree with the input data word and the error light can be reset to the off state by depressing the Error Reset pushbutton. The Detector Balance control permits the detector bridge circuit to be balanced to allow for differences in various detectors used. The Detector Threshold control provides a means of setting the detector threshold voltage above the noise and below the peaks of detector output voltage pulses for various detector output signal and noise conditions. The test points are used to monitor the following: Ground, Clock Pulse, Address Coincidence, Memory Output, Splitter Phase, Annihilator Phase, Detector Output, and Memory Timing Frame Sync. Completion and delivery of this exerciser is planned for the next quarter.

3. SUMMARY OF THE STATUS OF THIS PROGRAM

Since the last report, major advances in bubble domain device technology have been realized in the development of improved circuit components on in-house and other programs. In addition, a more complete understanding of the bubble domain device physics has been obtained which will provide the basis for rapid progress in device design in the future. Based on these device advances, further improvements in the required electronics have been made on this program.

Less spectacular, but quite important to the development of useful bubble domain devices, has been the identification of imperfections in garnet substrate crystals and their relationship to crystal growth parameters.

Improvement in substrate quality has not progressed as rapidly as hoped so that it has not been possible to carry out the desired experiments with GaYIG. Thus, other bubble domain materials which have useful properties will be employed for device work.

LITERATURE CITED

1. D. M. Heinz, J. L. Archer, P. J. Besser, P. E. Elkins, B. J. Huffman, J. E. Mee, L. A. Moudy and L. R. Tocci, "Single Crystal Orthoferrites for Memory Applications," Annual Summary Report, ECOM-0258-2, February 1972.

2. P. J. Besser, J. E. Mee, H. L. Glass, D. M. Heinz, S. B. Austerman, P. E. Elkins, T. N. Hamilton and E. C. Whitcomb, AIP Conf. Proc. 5, 125 (1972).

3. C. D. Brandle, D. C. Miller and J. W. Nielsen, J. Cryst. Growth 12, 195 (1972).

4. H. L. Glass, Mat. Res. Bull. 7, 385 (1972).

5. R. F. Belt, J. Appl. Phys. 40, 1644 (1969).

6. P. W. Shumate, Jr., IEEE Trans. Mag. 7, 586 (1971).

7. C. H. Hsin, T. J. Matcovich and R. L. Coren, AIP Conf. Proc. 5, 244 (1972).

8. Y. S. Lin, "Analysis of Permalloy Circuits for Bubble Domain Propagation," Intermag Conf., Kyoto, Japan, 1972, Paper 15.5.

9. J. L. Archer, L. R. Tocci, P. K. George and T. T. Chen, "Magnetic Bubble Domain Devices," Intermag Conf., Kyoto, Japan, 1972, Paper 58.2.

10. R. M. Goldstein and M. Shoji, AIP Conf. Proc. 5, 210 (1972).

11. W. F. Druyvesteyn, D. L. A. Tjaden and J. W. F. Dorleijn, "Calculation of the Stray Field of a Magnetic Bubble with Applications to Some Bubble Problems," (to be published in Philips Research Reports).

12. R. M. Goldstein and J. A. Copeland, J. Appl. Phys. 42, 2361 (1971).

13. J. A. Copeland, J. Appl. Phys. 43, 1905 (1972).

14. P. K. George and J. L. Archer, "Magnetization Distributions, Magnetostatic Energy Barriers, and Drive Fields for Permalloy Bars," (to be published in J. Appl. Phys.).

15. P. K. George and T. T. Chen, "Magnetostatic Potential Wells and Drive Field Access Bubble Domain Drive Circuits" (to be published in Appl. Phys. Letters).

16. P. K. George, "Drive Field Analysis of Field Access Bubble Domain Devices" (unpublished Technical Report NR T72-655/501).

17. P. I. Bonyhard, "System Requirements and Bubble Device Capabilities," Intermag Conf., Kyoto, Japan, 1972, Paper 58.1.

18. R. M. Sandfort and E. R. Burke, IEEE Trans. Mag. 7, 358 (1971).

19. H. N. Carlson, S. J. Perneski, L. F. Rago, G. J. Rothauser and W. D. P. Wagner, "Field Access Bubble to Bubble Logic Operations," Intermag Conf., Kyoto, Japan, 1972, Paper 15.1.

20. F. Yamauchi, K. Yoshimi, S. Fujiwara and T. Furuoya, "Bubble Switch and Circuit Utilizing YY Overlay," Intermag Conf., Kyoto, Japan, 1972, Paper 15.4.

21. A. H. Bobeck, R. F. Fischer and J. L. Smith, AIP Conf. Proc. 5, 45 (1972).

22. R. F. Fischer, IEEE Trans. Mag. 7, 741 (1971).

23. A. J. Perneski, IEEE Trans. Mag. 5, 554 (1969).

24. A. H. Bobeck, Symposium on Memory Materials and Devices, Princeton, May 1, 1972, Paper 3.

25. G. S. Almasi, B. J. Canavello, E. A. Giess, R. J. Hendel, R. E. Horstmann, T. F. Jamba, G. E. Keefe, J. V. Powers and L. L. Rosier, AIP Conf. Proc. 5, 220 (1972).

26. W. Strauss, P. W. Shumate, Jr. and F. J. Ciak, AIP Conf. Proc. 5, 235 (1972).

27. P. I. Bonyhard, I. Danylchuck, D. E. Kish and J. L. Smith, IEEE Trans. Mag. 6, 477 (1970).

APPENDIX A

SELECTED BIBLIOGRAPHY ON CYLINDRICAL MAGNETIC DOMAINS

A-1. CLASSIFICATION SYSTEM

The literature on Cylindrical Magnetic Domains presented in this Bibliography has been classified into the following categories:

1.   Theory of Cylindrical Magnetic Domains

2.   Materials

2.1   Orthoferrites

2.1.1 Orthoferrite Crystal Growth

2.1.2 Orthoferrite Material Properties

2.2   Garnets

2.2.1 Garnet Crystal Growth

2.2.2 Garnet Material Properties

2.3   Hexagonal Ferrites

2.4   Cobalt

3.   Device Aspects

3.1   Generation

3.2   Propagation

3.3   Detection

3.4   Devices

Each journal article in this compilation is listed under one or more of the above categories by the last name of the author (or of the first-named author if two or more names are involved) and the year of publication. Following the classification listings, the bibliography is assembled alphabetically by the same last name and year notation. Papers identified by a given author's name have been arranged chronologically by year of publication, irrespective of other names on the paper. Should more than one paper have been published by an author in a single year, the chronological sequence is designated by letters of the alphabet following the year, e.g., Thiele 1971b indicates the second paper authored by Thiele in 1971.

1. Theory of Cylindrical Magnetic Domains

Craik	1972	Dorleijn	1972
DeBonte	1972	Fowlis	1972
DeJonge	1972a	Hayashi	1972
DeJonge	1972b	Nelson	1972
Dimyan	1972		

2. Materials

2.1 Orthoferrites

Robbins	1972b

2.1.1 Orthoferrite Crystal Growth

Clover	1972	Okada	1971
Gyorgy	1971b	Pulliam	1971
Nakazumi	1971		

2.1.2 Orthoferrite Material Properties

Bobeck	1971c	Umebayashi	1971
Clover	1972	Varnerin	1971b
Hagedorn	1972	Yudin	1971
Hothersall	1972		
Lucas	1972		

2.2 Garnets

Robbins	1972b

2.2.1 Garnet Crystal Growth

Brandle	1972a	Pulliam	1972
Brandle	1972b	Quon	1972
Giess	1972	Robbins	1972a
Heinz	1972		

2.2.2 Garnet Material Properties

Argyle	1972	Kurtzig	1972a
Besser	1972	Kurtzig	1972b
Bobeck	1971c	LeCraw	1972
Bobeck	1972	Matthews	1972
Cronemeyer	1972	Pierce	1972
Dillon	1972	Quon	1972
Doyle	1972	Rosencwaig	1972a
Giess	1972	Rosencwaig	1972b
Glass	1972	Smith	1972
Hagedorn	1972	Stacy	1972
Heinz	1972	Sturge	1972a
Klokholm	1972	Sturge	1972b

44

2.3 Hexagonal Ferrites

2.4 Cobalt

Grundy   1972

3. Device Aspects

Almasi	1972a	Chang	1972
Almasi	1972b	Goldstein	1972
Bobeck	1972	Sadagopan	1972

3.1 Generation

Bobeck	1972	Chang	1972

3.2 Propagation

Argyle	1972	Goldstein	1972
Bobeck	1971c	Hagedorn	1972
Bobeck	1972	Hayashi	1972
Chang	1972	Hsin	1972
Copeland	1972a	Schlomann	1971
Copeland	1972b	Scholmann	1972
Fujiwara	1972	Slonczewski	1972

3.3 Detection

Bobeck	1972	Strauss	1972
Chang	1972	Yoshizawa	1972
Kataoka	1972		

3.4 Devices

Almasi	1972a	Hayashi	1972
Almasi	1972b	Shoji	1972
Bobeck	1972	Umebayashi	1971
Chang	1972		

A-2. BIBIOGRAPHY LISTINGS

Almasi 1972a

FABRICATION AND OPERATION OF A SELF-CONTAINED BUBBLE
DOMAIN MEMORY CHIP
G. S. Almasi, B. J. Canavello, E. A. Giess, R. J. Hendel,
R. E. Horstmann, T. F. Jamba, G. E. Keefe, J. V. Powers and
L. L. Rosier
AIP Conf. Proc. $\underline{5}$, 220 (1972).

Almasi 1972b

RELIABILITY AND ORGANIZATION OF A 10^8-BIT BUBBLE DOMAIN
MEMORY
G. S. Almasi, W. G. Bouricius and W. C. Carter
AIP Conf. Proc. $\underline{5}$, 225 (1972).

Argyle 1972

DOMAIN WALL MOTION IN RARE-EARTH SUBSTITUTED Ga:YIG
EPITAXIAL FILMS
B. E. Argyle, J. C. Slonczewski and A. F. Mayadas
AIP Conf. Proc. 5, 175 (1972).

Besser 1972

FILM/SUBSTRATE MATCHING REQUIREMENTS FOR BUBBLE DOMAIN
FORMATION IN CVD GARNET FILMS
P. J. Besser, J. E. Mee, H. L. Glass, D. M. Heinz, S. B. Austerman,
P. E. Elkins, T. N. Hamilton and E. C. Whitcomb
AIP Conf. Proc. 5, 125 (1972).

Bobeck 1971c

DYNAMIC PROPERTIES OF BUBBLE DOMAINS
A. H. Bobeck, I. Danylchuk, J. P. Remeika, L. G. Van Uitert and
E. M. Walters
Proc. Intern. Conf. Ferrites, Kyoto, 1970, Y. Hoshino, S. Iida and
M. Sugimoto, ed., University Park Press, Tokyo, 1971, pp 361-364.

Bobeck 1972

AN OVERVIEW OF MAGNETIC BUBBLE DOMAINS -- MATERIAL-DEVICE
INTERFACE
A. H. Bobeck, R. F. Fischer and J. L. Smith
AIP Conf. Proc. 5, 45 (1972).

Brandle 1972a

CZOCHRALSKI GROWTH OF RARE EARTH GALLIUM GARNETS
C. D. Brandle and A. J. Valentino
J. Cryst. Growth 12, 3 (1972).

Brandle 1972b

THE ELIMINATION OF DEFECTS IN CZOCHRANSKI GROWN RARE-EARTH
GALLIUM GARNETS
C. D. Brandle, D. C. Miller and J. W. Nielsen
J. Cryst. Growth 12, 195 (1972).

Chang 1972

A SELF-CONTAINED MAGNETIC BUBBLE DOMAIN MEMORY CHIP
H. Chang, J. Fox, D. Lu and L. L. Rosier
IEEE Trans. Mag. 8, 214 (1972).

Clover 1972

LOW BIREFRINGENT Sm-DOPED ORTHOFERRITES
R. B. Clover, M. Rayle and D. Gutman
AIP Conf. Proc. 5, 264 (1972).

Copeland 1972a

MAGNETIZATION OF SMALL PERMALLOY CIRCUIT ELEMENTS
J. A. Copeland
J. Appl. Phys. 43, 1905 (1972).

Copeland 1972b

THEORY OF SINGLE-CURRENT DOMAIN PROPAGATION CIRCUITS
J. A. Copeland
IEEE Trans. Mag. 8, 241 (1972).

Craik 1972

DERIVATION OF MAGNETIC PARAMETERS FROM DOMAIN THEORY
AND OBSERVATION
D. J. Craik and P. V. Cooper
J. Phys. D: Appl. Phys. 5 L37 (1972).

Cronemeyer 1972

ANNEALING OF LPE GARNET FILMS
D. C. Cronemeyer, E. A. Giess, E. Klotholm, B. E. Argyle and
T. S. Plaskett
AIP Conf. Proc. 5, 115 (1972).

DeBonte 1972

THEORY OF THE STATIC STABILITY OF THICK WALLED CYLINDRICAL
DOMAINS IN UNIAXIAL PLATELETS
W. J. DeBonte
AIP Conf. Proc. 5, 140 (1972).

DeJonge 1972a

MULTIPLE HYSTERESIS OF A HOLLOW CYLINDRICAL DOMAIN
F. A. DeJonge, W. D. Druyvesteyn and A. G. H. Veritulst
Intern. J. Magnetism 2, 7 (1972).

DeJonge 1972b

BUBBLE PHYSICS - STABILITY, DYNAMICS AND ANISOTROPY BUBBLE
LATTICES
F. A. DeJonge and W. F. Druyvesteyn
AIP Conf. Proc. 5, 130 (1972).

Dillon 1972

OPTICAL BIREFRINGENCE AND ANISOTROPY IN A UNIAXIAL
FERRIMAGNETIC GARNET
J. F. Dillon, Jr., E. M. Gyorgy and J. P. Remeika
AIP Conf. Proc. 5, 190 (1972).

Dimyan 1972

TEMPERATURE SENSITIVITY OF BUBBLE DOMAINS
D. Y. Dimyan and E. Della Torre
J. Appl. Phys. 43, 1285 (1972).

Dorcleijn 1972

MUTUAL INTERACTION BETWEEN BUBBLES IN DIFFERENT SHEETS
J. W. F. Dorleijn and W. F. Druyvesteyn
AIP Conf. Proc. 5, 135 (1972).

Doyle 1972

THE MAGNETIC ANISOTROPY IN POLISHED GdIG PLATELETS
W. D. Doyle
AIP Conf. Proc. 5, 707 (1972).

Fowlis 1972

RAPID METHOD FOR DETERMINING THE MAGNETIZATION AND
INTRINSIC LENGTH OF MAGNETIC BUBBLE DOMAIN MATERIALS
D. C. Fowlis and J. A. Copeland
AIP Conf. Proc. 5, 240 (1972).

Fujiwara 1972

BUBBLE DOMAIN DYNAMICS
S. Fujiwara, K. Yoshimi and T. Furuoya
AIP Conf. Proc. 5, 165 (1972).

Giess 1972

EUROPIUM-YTTRIUM IRON-GALLIUM GARNET FILMS GROWN BY
LIQUID PHASE EPITAXY ON GADOLINIUM GALLIUM GARNET
E. A. Giess, B. E. Argyle, D. C. Cronomeyer, E. Klokholm,
T. R. McGuire, D. F. O'Kane, T. S. Plaskett and V. Sadagopan
AIP Conf. Proc. 5, 110 (1972).

Glass 1972

X-RAY DOUBLE CRYSTAL TOPOGRAPHY OF EPITAXIAL MAGNETIC
BUBBLE DOMAIN GARNETS
H. L. Glass
Mat. Res. Bull. 7, 385 (1972).

Goldstein 1972

FUNCTIONAL BUBBLE DOMAIN CIRCUITS EMPLOYING BUBBLE-BUBBLE
INTERACTIONS
R. M. Goldstein and M. Shoji
AIP Conf. Proc. 5, 210 (1972).

Grundy 1972

THE EFFECT OF TEMPERATURE ON THE STABILITY OF BUBBLE
DOMAINS IN COBALT
P. J. Grundy, D. C. Hothersall and G. A. Jones
AIP Conf. Proc. 5, 155 (1972).

Gyorgy 1971b

COBALT SUBSTITUTED RARE EARTH ORTHOFERRITES
E. M. Gyorgy and L. G. Van Uitert
Proc. Intern. Conf. Ferrites, Kyoto, 1970, Y. Hoshino, S. Iida and
M. Sugimoto, ed., University Park Press, Tokyo, 1971, pp. 376-379.

Hagedorn 1972

DOMAIN WALL MOTION IN BUBBLE DOMAIN MATERIALS
F. B. Hagedorn
AIP Conf. Proc. 5, 72 (1972).

Hayashi 1972

AN ANALYSIS OF A CLEAR-VIEW ANGLEFISH BUBBLE-DOMAIN SHIFT
REGISTER

N. Hayashi, H. Chang, L. T. Romankiw and S. Krongelb
IEEE Trans. Mag. 8, 16 (1972).

Heinz 1972

BUBBLE DOMAINS IN CVD FILMS OF GALLIUM-SUBSTITUTED ERBIUM
IRON GARNET
D. M. Heinz, P. J. Besser and J. E. Mee
AIP Conf. Proc. 5, 96 (1972).

Hothersall 1972

THE DETECTION OF BUBBLE DOMAINS IN $YFeO_3$ BY SCANNING
ELECTRON MICROSCOPY
D. C. Hothersall, G. A. Jones and P. J. Grundy
J. Phys. D:Appl. Phys. 5, 440 (1972).

Hsin 1972

MEASUREMENTS OF BUBBLE DRIVE FIELDS IN A T-BAR CONFIGURATION
C. H. Hsin, T. J. Matcovich and R. L. Coren
AIP Conf. Proc. 5, 244 (1972).

Kataoka 1972

SEMICONDUCTOR FUNCTIONAL ARRAYED DETECTOR FOR MAGNETIC-
BUBBLE DOMAINS
S. Kataoka, H. Yamada, S. Iida and Y. Sugiyama
Proc. IEEE 60, 460 (1972).

Klokholm 1972

EPITAXIAL STRAINS AND FRACTURE IN GARNET FILMS
E. Klokholm, J. W. Matthews, A. F. Mayadas and J. Angilello
AIP Conf. Proc. 5, 105 (1972).

Kurtzig 1972a

CORRELATION OF DOMAIN WALL MOBILITY WITH GALLIUM
CONCENTRATION IN BUBBLE GARNETS
A. J. Kurtzig, R. C. LeCraw, A. H. Bobeck, E. M. Walters, R. Wolfe,
H. J. Levinstein and S. J. Licht
AIP Conf. Proc. 5, 180 (1972).

Kurtzig 1972b

CONTROL OF THE MAGNETIZATION OF BUBBLE GARNETS BY
ANNEALING
A. J. Kurtzig and M. Dixon
J. Appl. Phys. 43, 2883 (1972).

LeCraw 1972

TEMPERATURE DEPENDENCE OF GROWTH-INDUCED MAGNETIC
ANISOTROPY IN EPITAXIAL GARNET FILMS BY RESONANCE
TECHNIQUES
R. C. LeCraw and R. D. Pierce
AIP Conf. Proc. 5, 200 (1972).

Lucas 1972

SELF-BIASED BUBBLES IN YTTERBIUM ORTHOFERRITE PLATELETS
J. M. Lucas and P. P. Luff
AIP Conf. Proc. 5, 145 (1972).

Matthews 1972

FRACTURE OF BRITTLE EPITAXIAL FILMS UNDER THE INFLUENCE
OF MISFIT STRESS
J. W. Matthews and E. Klokholm
Mat. Res. Bull. 7, 213 (1972).

Nakazumi 1971

GROWTH OF SINGLE CRYSTALS OF RARE EARTH ORTHOFERRITES
BY THE VERNEUIL METHOD
Y. Nakazumi, K. Daido, I. Tsuboya and M. Saito
Proc. Intern. Conf. Ferrites, Kyoto, 1970, Y. Hoshino, S. Iida and
M. Sugimoto, ed., University Park Press, Tokyo, 1971, pp. 306-309.

Nelson 1972

STABLE REVERSAL DOMAINS IN THIN FILM STRIPS
T. J. Nelson and Y. S. Chen
AIP Conf. Proc. 5, 150 (1972).

Okada 1971

PREPARATION OF ORTHOFERRITE SINGLE CRYSTALS BY THE
FLOATING ZONE TECHNIQUE
T. Okada, K. Matsumi and H. Makino
Proc. Intern. Conf. Ferrites, Kyoto, 1970, Y. Hoshino, S. Iida and
M. Sugimoto, ed., University Park Press, Tokyo, 1971, pp. 372-375.

Pierce 1972

CRYSTALLOGRAPHIC CONSIDERATIONS IN THE USE OF CUBIC
MATERIALS WITH INDUCED ANISOTROPIES IN BUBBLE DOMAIN
DEVICES
R. D. Pierce
AIP Conf. Proc. 5, 91 (1972).

Pulliam 1971

FORMATION AND CHARACTERIZATION OF EPITAXIAL MAGNETIC
OXIDE FILMS
G. R. Pulliam, J. E. Mee, D. M. Heinz, P. J. Besser and J. H. Collins
Proc. Intern. Conf. Ferrites, Kyoto, 1970, Y. Hoshino, S. Iida and
M. Sugimoto, ed., University Park Press, Tokyo, 1971, pp. 314-317.

Quon 1972

GROWTH OF SINGLE CRYSTAL RARE-EARTH GARNET FILMS BY
LIQUID PHASE EPITAXY
H. H. Quon and A. J. Potvin
Mat. Res. Bull. 7, 463 (1972).

51

Robbins 1972a

THE GROWTH OF EPITAXIAL GARNET FILMS FROM COPRECIPITATED
GARNET-FLUX SOLUTIONS
M. Robbins, S. J. Licht and H. J. Levinstein
AIP Conf. Proc. 5, 101 (1972).

Robbins 1972b

PREPARATION OF POLYCRYSTALLINE RARE EARTH ORTHOFERRITES
AND GARNETS VIA HYDROXIDE PRECIPITATION
M. Robbins, G. K. Wertheim, A. R. Storm and D. N. E. Buchanan
Mat. Res. Bull. 7, 233 (1972).

Rosencwaig 1972a

GROWTH-INDUCED MAGNETIC ANISOTROPY IN EPITAXIAL GARNET
FILMS
A. Rosencwaig and W. J. Tabor
Appl. Phys. Lett. 20, 40 (1972).

Rosencwaig 1972b

GROWTH-INDUCED NONCUBIC ANISOTROPY IN BUBBLE GARNETS
A. Rosencwaig and W. J. Tabor
AIP Conf. Proc. 5, 57 (1972).

Sadagopan 1972

HIGH-DENSITY BUBBLE DOMAIN SHIFT REGISTER
V. Sadagopan, M. Hatzakis, K. Y. Ahn, T. S. Plaskett and L. L. Rosier
AIP Conf. Proc. 5, 215 (1972).

Schlomann 1972

STRUCTURE OF MOVING DOMAIN WALLS IN MAGNETIC MATERIALS
E. Schlomann
Appl. Phys. Lett. 19, 274 (1971).

Schlomann 1972

STRUCTURE AND ENERGY OF MOVING DOMAIN WALLS
E. Schlomann
AIP Conf. Proc. 5, 160 (1972).

Shoji 1972

MAGNETIC BUBBLE COUNTING CIRCUITS
M. Shoji
IEEE Trans. Mag. 8, 240 (1972).

Slonczewski 1972

DYNAMICS OF MAGNETIC DOMAIN WALLS
J. C. Slonczewski
AIP Conf. Proc. 5, 170 (1972).

Smith 1972

THE TEMPERATURE DEPENDENCE OF BUBBLE PARAMETERS IN
SOME RARE-EARTH GARNET FILMS
D. H. Smith and A. W. Anderson
AIP Conf. Proc. 5, 120 (1972).

Stacy 1972

GROWTH INDUCED MAGNETIC ANISOTROPY IN YTTRIUM IRON GARNET
W. T. Stacy
AIP Conf. Proc. 5, 185 (1972).

Strauss 1972

MAGNETORESISTANCE SENSORS FOR GARNET BUBBLE DOMAINS
W. Strauss, P. W. Shumate, Jr. and F. J. Ciak
AIP Conf. Proc. 5, 235 (1972).

Sturge 1972a

DICHROISM DUE TO SITE SELECTIVITY OF RARE EARTH IONS IN
GARNETS
M. D. Sturge and J. P. van der Ziel
AIP Conf. Proc. 5, 195 (1972).

Sturge 1972b

MICROSCOPIC THEORY OF THE GROWTH-INDUCED ANISOTROPY OF
YGdFe GARNET
M. D. Sturge
AIP Conf. Proc. 5, 205 (1972).

Umebayashi 1971

CONTROLLABLE DOMAIN PATTERN PRINTING EFFECT IN $YFeO_3$
H. Umebayashi and K. Ono
Proc. Intern. Conf. Ferrites, Kyoto, 1970, Y. Hoshino, S. Iida and
M. Sugimoto, ed., University Park Press, Tokyo, 1971, pp. 365-367.

Varnerin 1971b

DEFECT AND GROWTH CONSIDERATIONS IN MAGNETIC BUBBLE
DOMAIN MATERIALS
L. J. Varnerin, Jr.
Proc. Intern. Conf. Ferrites, Kyoto, 1970, Y. Hoshino, S. Iida and
M. Sugimoto, ed., University Park Press, Tokyo, 1971, pp. 368-371.

Yoshizawa 1972

DETECTION OF BUBBLE DOMAINS BY HALL EFFECT OF
EVAPORATED INDIUM ANTIMONIDE
S. Yoshizawa, T. Oi, J. Shigeta, I. Mikami and G. Kamoshita
AIP Conf. Proc. $\underline{5}$, 230 (1972).

Yudin 1971

WALL MOTION AND STABILITY OF CYLINDRICAL DOMAINS IN
FERRITES
V. M. Yudin and T. A. Fomina
Sov. Phys.-Solid State $\underline{14}$, 1234 (1971).